THESIS

NUMERICAL MODELING AND HYDROCHEMICAL ANALYSIS OF THE CURRENT AND FUTURE STATE OF SEAWATER INTRUSION IN THE TODOS SANTOS AQUIFER, MEXICO

Submitted by

Marissa M. Fichera

Department of Geosciences

In partial fulfillment of the requirements

For the Degree of Master of Science

Colorado State University

Fort Collins, Colorado

Spring 2019

Master's Committee:

Advisor: William E. Sanford

Michael J. Ronayne
Ryan T. Bailey

ABSTRACT

NUMERICAL MODELING AND HYDROCHEMICAL ANALYSIS OF THE CURRENT AND FUTURE STATE OF SEAWATER INTRUSION IN THE TODOS SANTOS AQUIFER, MEXICO

The Todos Santos aquifer, Baja California Sur, Mexico, provides the sole source of freshwater to the town of Todos Santos, and is utilized for domestic and agricultural needs crucial to the town's economy. The region is characterized by an arid climate. Major recharge to the aquifer is supplied from intermittent cyclones. Irregular and unpredictable recharge rates combined with population growth resulting from resort development put the Todos Santos aquifer at risk of overexploitation, causing potentially permanent water quality degradation by salinization as a result of seawater intrusion.

Understanding the complex response of seawater intrusion to variable pumping rates and sea-level rise is critical to water resource management in Todos Santos. This study utilized numerical simulation of variable-density groundwater flow, using SEAWAT, in conjunction with temporal and spatial hydrochemical analysis, to evaluate the current and future extent of seawater intrusion in the area. Forecasting simulations were run for five, ten, and twenty years following 2017, for five different hydrologic scenarios, which implemented various pumping rates, sea-level rise, and overexploitation of significant surface water resources.

Hydrochemical analysis shows an increase in groundwater specific conductance and chloride concentration within two kilometers of the coastline from 2007 to 2017. This combined with the distribution of groundwater samples exhibiting chloride concentration above the

permissible limit for potable water (250 mg/L) suggest that the Todos Santos aquifer is experiencing effects of seawater intrusion up to 1.6 kilometers inland as of 2017. Analysis of groundwater cation exchange reactions indicates widening of the freshwater-seawater mixing zone from 2007 to 2017, further suggesting the exacerbation of seawater intrusion over this time span. Forecasting simulation results indicate that the extent of seawater intrusion is exacerbated by increased water withdrawal, overexploitation of surface water resources, the current rate of sea-level rise (~ 4 mm/yr), and an increased rate of sea-level rise of 25 mm/yr.

ACKNOWLEDGMENTS

I would like to express my sincere appreciation for my advisor, Dr. William Sanford, for his consistent academic support and for facilitating my understanding of groundwater flow processes over the past few years. I have been very fortunate to work with someone I get along with so well, and who has been patient and understanding with me throughout this process.

I honestly cannot thank Dr. Mike Ronayne enough for always leaving his door open! From the initial model setup to the final write-up, he has been there to answer any and every groundwater modeling inquiry I've had. I am also grateful for Dr. Ryan Bailey for his contributions to my thesis committee, as well as his PhD student, Mosaed Alrashidi, for his invaluable assistance in navigating SEAWAT.

I would like to thank CONAGUA La Paz, specifically Edda Loera and Luis Meza, and Antonio for their assistance in sample collection and analysis in March and June of 2017. I'd also like to thank the director of the Colorado State University Todos Santos Center, Aines Castro, for her assistance in numerous aspects, both during my time in Todos Santos and throughout the entirety of the project. I'd also like to express additional thanks to Andrea Purdy, CSU Professor of Spanish, for always facilitating communication across language barriers both in the field and through electronic communication!

I would like to thank my parents, Marianne and Sebastian, for their patience, acceptance, and unrelenting support of both my academic and non-academic goals. My final thanks goes to the graduate student community here at CSU, including Michael Baker for his patience and wonderfully concise answers to every math, physics, and MATLAB question I've ever had, and to Amanda Doherty, Andrew McCarthy, and Nikki Seymour.

TABLE OF CONTENTS

LIST OF TABLES

Table 11: Transient 2007-2017 mass balance summary. Mass balance results are presented for final flow time steps (time step 6) corresponding to final growing and non-growing stress periods (stress periods 20 and 19, respectively).

Table 12: Simulated seawater-freshwater interface model results for steady-state, transient (’07-’17), and forecasting scenarios for 5, 10, and 20 years. Results are listed for the following locations: (a) Todos Santos town area, and (b) Punta Lobos beach (Fig. 6), and for the following scenarios: (1) Pumping rates remain at 2007 conditions, (2) Pumping rates are doubled in all wells, (3) Pumping rates remain at 2017 conditions, sea-level rise of 4 mm/yr, (4) Pumping rates remain at 2017 conditions, Arroyo La Reforma is overexploited in lower reaches, and (5) Pumping rates remain at 2017 conditions, sea-level rise of 25 mm/yr.

LIST OF FIGURES

CHAPTER 1

INTRODUCTION

Globally, communities relying on freshwater supply from coastal aquifers have been and continue to be at risk of being significantly impacted by seawater intrusion. Coastal areas are the most densely populated areas in the world, with half of the world's population living in coastal regions (Post, 2005). Water resource management problems arise especially in arid to semi-arid regions, where groundwater is the sole source of freshwater, and precipitation accumulation is generally low and unpredictable. Climate change and sea level rise threaten to worsen this effect. Tourism and agriculture also play a role in high water demand, with seasonal population increase induced by expanding resort developments and demand for water-intensive crops leading to potential increase in groundwater extraction. While overexploitation of groundwater resources is a cause for concern in any region, coastal aquifers are unique in that overexploitation puts them at risk of seawater intrusion.

The volume of research pertaining to the topic of seawater intrusion illustrates just how much of a global phenomenon it is. Post (2005) lists numerous well documented cases of seawater intrusion problems around the world, including Hawaiian, Floridian, Atlantic and Gulf coastal plains in the United States (Konikow and Reilly, 1999), Mediterranean coastal aquifers (Lopez-Geta et al., 2003), at least 100 areas in Europe (Scheidleder & Grath, 2004), and The Netherlands (Kooiman, Stuyfzand, Maas, & Kappelhof, 2004). Further studies of seawater intrusion have been applied to agricultural arid coastal regions in Oman (Walther et al., 2012), the Alabama Gulf Coast in the United States (Lin et al., 2008), an irrigation area in Queensland,

Australia (Narayan et al., 2007), coastal areas in Libya (Alfarrah & Walraevens, 2018), and coastal aquifers in the south coast of Laizhou Bay, China (Chang et al., 2018).

Mexico specifically, with over 9,000 km of coastline and 17 states along the coast, has been the subject of this increased risk, with 10 of the 17 coastal states having experienced seawater intrusion by 1993 (Cardoso, 1993). Baja California Sur (BCS), Mexico has 12 coastal aquifers bordering the Pacific Ocean and Gulf of California, six of which experienced seawater intrusion as early as 1980 (Cardoso, 1993). Cardoso also states the southwest region of BCS, an area which encompasses multiple aquifers bordering the Pacific Ocean, including the Todos Santos Aquifer, was designated as overexploited in 1993. Additional studies have been done on processes which contribute to seawater intrusion in regions that reside north of Todos Santos in BCS, including La Paz (Tamez-Meléndez et al., 2016) and Santo Domingo (Cardona et al., 2004).

Todos Santos (Fig. 1) is a coastal town in Baja California Sur, Mexico, located approximately 70 km north of Cabo San Lucas and 80 km southwest of the state's capitol, La Paz. The town's coastal location and temperate climate have contributed to a growing tourism market and extensive agriculture in the area, leading to an increased demand for water supply. The Todos Santos Aquifer is the town's sole source of freshwater, and is utilized for both domestic and agricultural use. Increasing demand for freshwater is putting the aquifer at risk of overexploitation, and consequently seawater intrusion and water quality degradation by salinization. This study aims to analyze spatial and temporal changes in water quality of the Todos Santos Aquifer over a ten year period from 2007 to 2017, and utilize groundwater modeling to predict the extent of seawater intrusion as a consequence of increased groundwater extraction and sea level rise. Various field data was compiled from the Comisión Nacional del

Agua's (CONAGUA) study of BCS aquifers (2007) and from field investigations conducted in June of 2017 to analyze changes in water quality. A numerical model of variable-density groundwater flow was developed using USGS's SEAWAT code (Langevin et al., 2008) to investigate the extent of seawater intrusion in the Todos Santos Aquifer over timescales of 5, 10, and 20 years post-2017. Predictive simulations include increased pumping, sea-level rise, and over-exploitation of surface water resources. Numerical simulation results combined with temporal and spatial water quality analysis are intended to provide Todos Santos with useful information in management of water resources.

CHAPTER 2

BACKGROUND

2.1 Area of Study

Todos Santos is located on the southwestern portion of Baja California Sur, Mexico, between the Sierra De La Laguna mountain range and the Pacific Ocean (Fig. 1). It has a population of 6,485 people as of 2015 (INEGI, 2015). Drivers of economic growth for the town include agriculture and a growing tourism market. The Todos Santos Aquifer is the town's sole source of freshwater.

2.2 Climate

Todos Santos lies directly on the Tropic of Cancer, tending to an arid climate. Average annual temperatures range from 15.4°C to 27.3°C, with a mean annual temperature of 21.3°C (Tres Santos, 2012). The region is characterized by prolonged droughts interrupted by abrupt storms in the form of cyclones, which provide most of the area's precipitation, and occur during the summer months. The mean annual precipitation is 150.2 mm, however, recorded annual precipitation values ranged from 8.5 mm to 404 mm between 1961 and 2011 (Tres Santos, 2012).

2.3 Agriculture

Temperate climate and an oasis ecosystem allow Todos Santos to economically depend on farming of a variety of crops. The majority of crops are grown during the autumn-winter cycle (September-February) with very few being grown during the spring-summer cycle (Tres

Santos, 2012). Poblano peppers are the main crop planted, comprising 41% of the region's irrigated area (Ceseña, 2015). Other crops of economic significance include basil, green beans, and culinary herbs, comprising 17%, 16%, and 10% of the region's irrigated area, respectively (Ceseña, 2015). Crops of minor significance include cucumber and tomatoes, along with tropical fruit trees such as mangos, avocados, papayas, guavas, and citrus. A total of 670 hectares (1655 acres) were planted in Todos Santos during the autumn-winter cycle from 2014-2015 (SAGARPA, 2015).

2.4 Geologic Background

Bedrock in the region of interest is comprised of igneous and metamorphic rock types, including granite, granodiorite, gabbro, metasandstone, amphibolite, and phyllite (Calera et al., 2001). Jurassic-aged metasandstone crops out in isolated portions as cliffs on the Todos Santos coastline. The Sierra De La Laguna mountain range, comprised of mid to late Cretaceous-aged granodiorite and granite, trends roughly north-south for approximately 80 kilometers in the south-central portion of Baja California Sur and reaches altitudes of over 2,000 meters above sea level. Uplift of these mountains occurred approximately 20 Ma, resulting in a horst and graben structural setting. Erosion of the mountain range filled the Todos Santos valley with alluvial sediments primarily composed of polymict conglomeratic sand (Tres Santos, 2012).

2.5 Aquifer Description

The Todos Santos Aquifer extent as delineated by The National Water Commission of Mexico, abbreviated CONAGUA, is shown in Figure 1. This aquifer encompasses an area of approximately 200 square kilometers, and is bordered by the Canada Honda Aquifer to the north and the Pescadero Aquifer to the south. The Sierra De La Laguna Mountains to the northeast

create a watershed divide between the east and west coasts of the Baja Peninsula. Aquifer material is comprised of Tertiary and Quaternary alluvial sediments in a basin-fill geometry of unknown thickness. Igneous and metamorphic bedrock bounds the extent of alluvial sediments at depth, however, intense faulting and fracturing of this bedrock is thought to provide conduits to flow. Transmissivity values range from 1.31 to 84.78 $\times 10^{-3}$ m^2/s (CONAGUA, 2007).

The main surface water catchment corresponds to Arroyo La Reforma (Fig. 1), which flows roughly northeast to southwest from the Sierra De La Laguna Mountains and discharges into the ocean (depending on water supply). A reservoir created by Santa Ines Dam exists just north of the aquifer boundary, and provides flow to La Reforma (Tres Santos, 2012). Runoff into La Reforma from high-altitude precipitation is either discharged into the ocean or infiltrates into the aquifer. Most domestic and irrigation wells are located in close proximity to La Reforma.

Additional surface water features include natural springs, and most notably the La Poza estuary, located approximately 150 meters off the coastline due east of Todos Santos (Fig. 1). Consisting of a delicate balance of freshwater and seawater, La Poza provides a unique habitat to over 100 species of birds and insects, many of which are endemic to only Baja California Sur (Carmona et al., 2017). However, notable decreasing areal extent and declining biodiversity has prompted local concern that previously observed freshwater influx has been diverted, and that the freshwater-seawater balance has been severely disrupted.

Hydraulic head data published in 2007 indicate a general northeast to southwest groundwater flow direction that follows the topography (CONAGUA, 2007). Recharge is believed to originate in higher-elevation areas, and groundwater is discharged by way of groundwater extraction via pumping or into the ocean. It is estimated that only 6 mm of annual

precipitation reaches to recharge the aquifer, and the remainder is evaporated or arrives by runoff into the ocean (Carmona et al., 2017).

2.6 Previous Work

There have been numerous water balance studies done on the aquifers of Baja California Sur. Because the area is subject to extreme droughts interrupted by large storms, groundwater availability varies between studies. In 2009, the Todos Santos aquifer showed an annual deficit of 151,030 m^3, whereas in 2015 it was shown to be in balance (Federman, 2015).

CONAGUA (2007) published a comprehensive study of five aquifers on the Pacific coast of Baja California Sur, and found the amount of available groundwater in the Todos Santos aquifer to be ~ 500,000 m^3. A significant amount of data was compiled from this 2007 study for the purposes of the current study's spatial and temporal water quality analysis, and additionally aided significantly in numerical model construction. Data published in 2007 (Table 1) utilized in the current study includes well locations, pumping rates and durations, spring locations, hydraulic head measurements, and measurements of specific conductance and major ions. CONAGUA collected a total of 36 water samples. 12 hydraulic head measurements and 27 specific conductance measurements were published, as well as major ion analysis for 12 samples (Table 1). Sample locations are displayed in Figure 2.

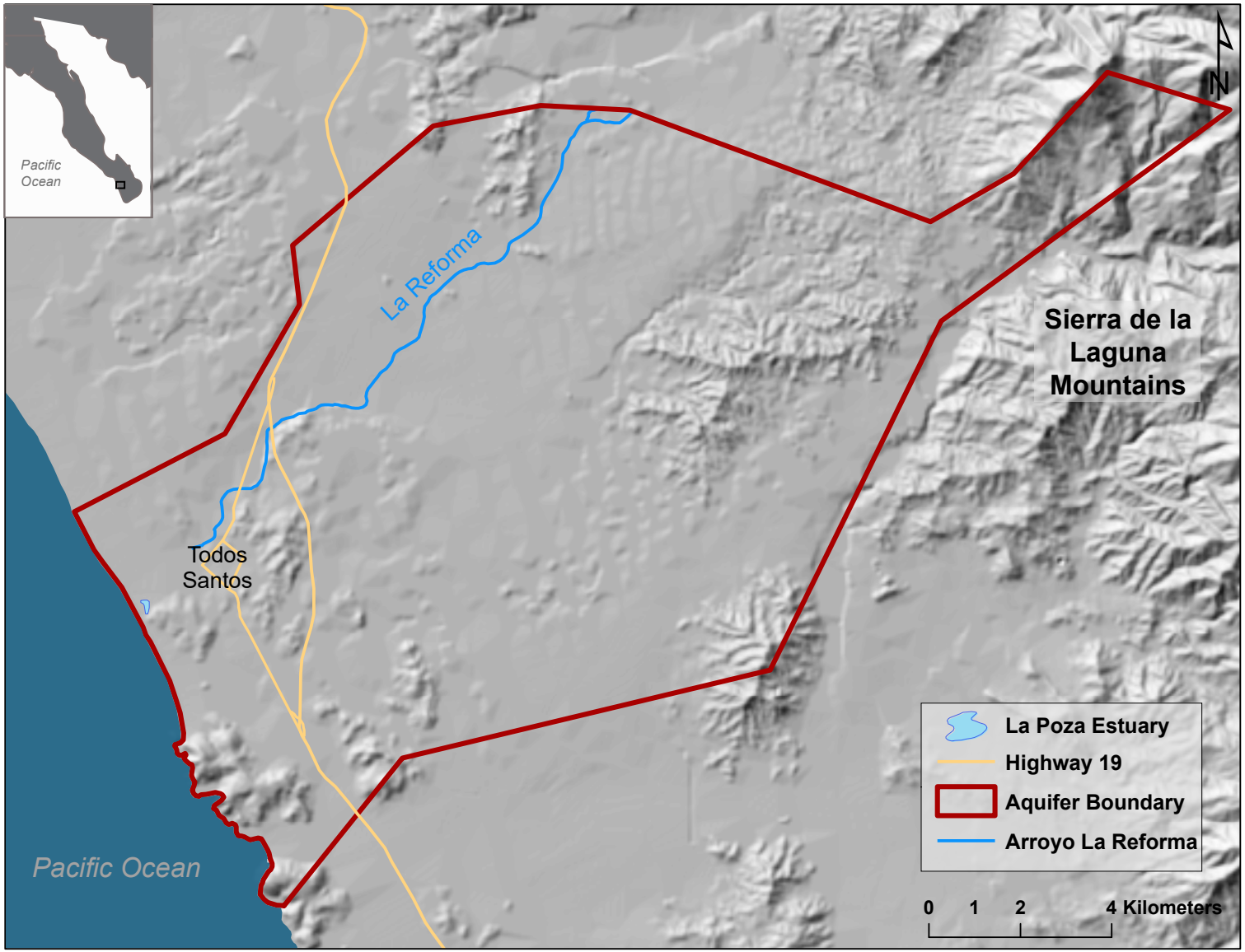

Figure 1: Area of aquifer study within Baja California Sur, Mexico. Aquifer extent is delinated by CONAGUA. Arroyo La Reforma is the main surface water catchment in the area. La Poza is a small estuary located southeast of town.

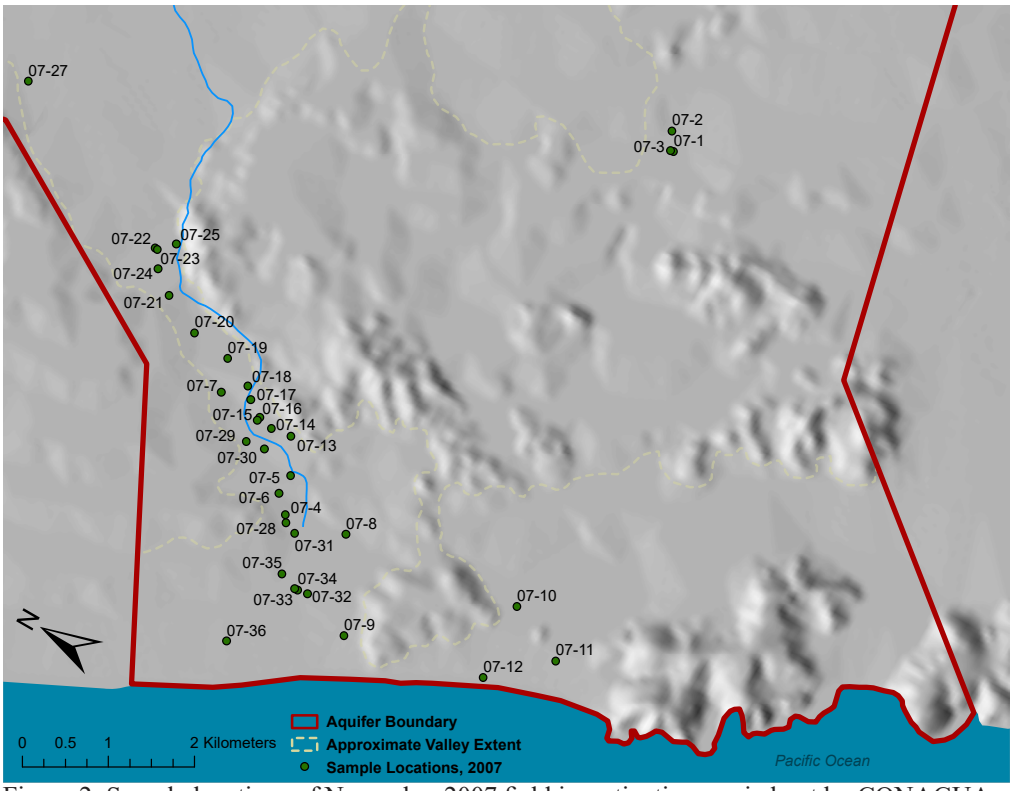

Figure 2: Sample locations of November 2007 field investigation carried out by CONAGUA. Interpreted extent of the Todos Santos valley is shown.

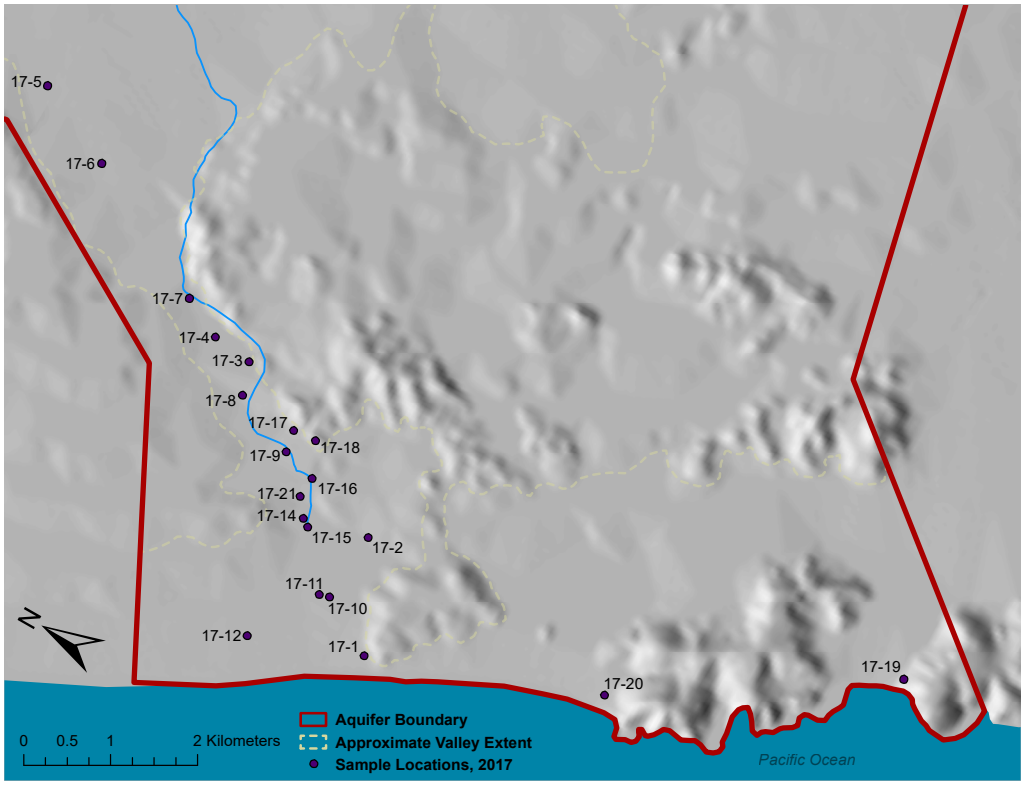

Figure 3: Sample locations of June 2017 field investigation.

Table 1: Field data collected in 2007 (CONAGUA) and 2017, and corresponding major ion analysis results. Stable isotope analysis results are included for 2017 (unavailable for 2007).

Sample	COORDINATES UTM ZONE 12Q		Date	Temp. (°C)	pH	Specific Conductance (µS/cm)	Ca^{2+}	Mg^{2+}	Na^{+}	K^{+}	Cl^{-}	HCO_3^{-}	SO_4^{2-}		
	Northing (m)	Easting (m)					(mg/L)								
1	2592040	584642	05/11/07	24.7	5.48	2462.0	112	59.3	346.83	6.85	629.2	700	117.57		
2	2592175	584841	06/11/07	23.7	6.35	1326.0	-	-	-	-	-	-	-		
3	2592079	584634	06/11/07	22.1	6.00	2287.0	-	-	-	-	-	-	-		
4	2593836	578736	07/11/07	26.3	7.05	724.0	59.1	20.9	66.67	6.55	111.7	220	59.47		
5	2594011	579159	07/11/07	-	-	-	-	-	-	-	-	-	-		
6	2594027	578913	07/11/07	-	-	-	-	-	-	-	-	-	-		
7	2595193	579595	07/11/07	-	-	-	-	-	-	-	-	-	-		
8	2593116	578891	13/11/07	22.3	6.93	1037.0	46.7	37.6	118.84	13.99	180.8	380	20.31		
9	2592546	577859	13/11/07	22.9	7.05	718.0	66.9	18.9	60.87	4.17	113.4	220	55.71		
10	2590973	579158	13/11/07	-	-	-	-	-	-	-	-	-	-		
11	2590267	578836	13/11/07	-	-	-	-	-	-	-	-	-	-		
12	2590901	578247	13/11/07	-	-	-	-	-	-	-	-	-	-		
13	2594235	579557	13/11/07	25.6	6.22	659.0	29.5	18.7	60.87	5.06	69.1	200	15.4		
14	2594478	579524	13/11/07	25.3	6.58	601.0	-	-	-	-	-	-	-		
15	2594663	579543	13/11/07	25.6	6.45	600.0	-	-	-	-	-	-	-		
16	2594660	579538	13/11/07	25.3	6.84	608.0	-	-	-	-	-	-	-		
17	2594855	579693	13/11/07	26.0	6.46	590.0	-	-	-	-	-	-	-		
18	2594962	579812	13/11/07	25.8	7.12	569.0	38.9	19.9	46.38	3.57	79.8	280	29.82		
19	2595326	579974	13/11/07	27.3	6.27	1664.0	-	-	-	-	-	-	-		
20	2595807	580037	13/11/07	25.4	6.60	390.0	24.9	9.6	29.09	2.78	21.3	200	5.68		
21	2596279	580265	13/11/07	25.2	6.70	324.0	-	-	-	-	-	-	-		
22	2596697	580662	13/11/07	-	-	-	-	-	-	-	-	-	-		
23	2596686	580665	13/11/07	-	-	-	-	-	-	-	-	-	-		
24	2596547	580468	14/11/07	25.8	6.80	794.0	-	-	-	-	-	-	-		
25	2596507	580824	14/11/07	27.7*	6.72	1550.0	116.6	36.3	163.01	5.23	381.1	300	27.62		
26	2597948	575320	14/11/07	26.5	7.52	381.0	23.3	9.7	28.6	2.22	46.1	120	9.79		
27	2598939	581603	14/11/07	24.1	7.18	308.0	-	-	-	-	-	-	-		
28	2593784	578658	14/11/07	26.7	6.95	954.0	-	-	-	-	-	-	-		
29	2594655	579247	14/11/07	25.6	7.21	509.0	-	-	-	-	-	-	-		
30	2594432	579276	14/11/07	25.2	7.00	612.0	-	-	-	-	-	-	-		
31	2593635	578602	14/11/07	25.5	7.32	777.0	-	-	-	-	-	-	-		
32	2593157	578070	15/11/07	24.9	6.93	755.0	62.2	23.6	61.69	3.91	113.4	220	49.31		
33	2593279	578050	15/11/07	23.9	6.80	879.0	-	-	-	-	-	-	-		
34	2593278	578050	15/11/07	-	-	-	-	-	-	-	-	-	-		
35	2593528	578120	15/11/07	24.7	6.90	869.0	68.4	18.9	65.2	4.29	124.1	260	16.67		
36	2593697	577123	15/11/07	26.6	6.96	1033.0	46.7	23	128.47	9.93	159.5	300	25.11		
														$\delta^{18}O$ ‰	$\delta^{2}H$ ‰
17-1	2592274	577734	13/6/7	27.0	7.74	74400.0	1523	3450	24825	632.9	32388.6	-	4187.9	8.50513	11.8099
17-2	2592919	578950	13/6/7	24.2	8.10	1307.0	67.7	29.865	82.6	7.13	216.896	273	61.45	-10.022	-68.775
17-3	2595130	580038	13/6/7	26.4	7.36	898.4	44.005	16.82	63.45	2.1855	136.975	159	33.789	-9.595	-66.846
17-4	2595610	580093	13/6/7	26.2	7.19	457.4	100.85	33.975	62	6.37	31.441	135	25.094	-10.719	-77.489
17-5	2598742	581660	13/6/7	25.1	7.52	390.9	87.05	27.145	55.25	5.59	27.354	131	15.358	-9.6141	-73.782
17-6	2597750	581187	13/6/7	26.5	7.27	456.4	99.4	31.1	71	5.995	41.823	136	19.386	-8.5375	-73.474
17-7	2596095	580333	13/6/7	25.9	7.43	429.1	100.05	32.07	66.4	6.135	36.438	132	18.621	-9.4855	-76.522
17-8	2594998	579661	13/6/7	26.6	7.14	604.2	42.355	13.59	28.45	1.6245	68.662	135	26.086	-8.3539	-74.892
17-9	2594237	579340	13/6/7	26.6	7.31	1159.0	77.5	25.315	64.55	2.6685	205.01	198	65.822	-7.616	-74.15
17-10	2592958	578129	14/6/17	25.9	6.94	1357.0	80.85	28.755	61.05	2.5985	205.655	226	57.997	-7.5624	-70.391
17-11	2593075	578096	14/6/17	25.4	6.91	1199.0	74.675	24.5125	57.1	1.86425	171.212	214	54.874	-7.7738	-70.474
17-12	2593553	577266	14/6/17	26.4	7.01	2505.0	156.3	69.61	132.9	13.39	549.244	305	213.1	-8.166	-71.353
17-13	2596977	575651	14/6/17	27.2	7.04	1318.0	53.95	24.135	114.8	1.6825	308.687	189	123.5	-8.2347	-72.411
17-14	2593677	578770	14/6/17	26.4	7.10	740.3	53.8	18.6	35.705	2.202	110.425	167	40.06	-8.8721	-75.308
17-15	2593583	578710	14/6/17	25.6	8.43	1188.0	71.15	25.16	66	2.801	215.707	178	70.752	-10.667	-72.955
17-16	2593821	579222	14/6/17	26.9	7.34	917.4	55.55	20.925	42.455	2.5065	111.814	183	42.015	-10.958	-72.054
17-17	2594285	579600	14/6/17	27.1	7.13	1077.0	53.65	19.85	70.1	2.5	186.539	161	45.476	-9.4491	-68.144
17-18	2594009	579622	14/6/17	26.9	7.45	1214.0	63.7	24.1	75.2	3.071	218.542	185	53.067	-10.105	-67.774
17-19	2586760	580601	15/6/17	21.4	6.95	1594.0	57.7	25.98	160.85	0.6025	428.813	229	61.795	-9.6141	-69.047
17-20	2589648	578722	15/6/17	27.2	7.34	4786.0	74.4	159.35	776.5	44.805	846.255	378	255.345	-11.646	-75.978
17-21	2593836	578975	15/6/17	25.3	6.83	932.5	65.575	23.4825	43.9675	2.30675	202.95	167	76.13	-11.949	-74.401

CHAPTER 3

METHODS

3.1 Hydrochemical Analysis

Field data, lab analysis, and groundwater modeling were implemented in analyzing the Todos Santos Aquifer. Two field investigations were conducted in March and June of 2017, resulting in the collection of 21 water samples. Samples were taken from domestic wells, irrigation wells, and various surface water sources. Surface water sources included springs and the La Poza estuary, as well as a wetland located inland of Las Palmas beach, a small area with a high concentration of palm trees on the southern end of the aquifer boundary. Sample locations are shown in Figure 3.

Samples were tested in the field to obtain temperature and specific conductance. Samples were then analyzed for major ions by CONAGUA, and for stable isotopes $\delta^{18}O$ and $\delta^{2}H$ at the Monterrey Institute of Technology and Higher Education in Mexico. Table 1 shows field data collected in June of 2017 and corresponding lab results. Stable isotope results were plotted with the Global Meteoric Water Line (Craig, 1961) to analyze groundwater recharge mechanisms (Fig. 4). Major ion results were analyzed in the form of Piper Diagrams and Hydrochemical Facies Evolution Diagrams (HFE-D) (Giménez-Forcada, 2010) and compared with major ion data published in 2007 by CONAGUA. Piper Diagrams were utilized to visualize the relative abundance of ions in water samples, and require plotting the major cation and anion composition of each sample on respective ternary diagrams. The two ternary diagrams are then projected onto a diamond representing various hydrochemical facies, utilized to determine groundwater type.

The HFE-D requires inputs of major ions, similar to the Piper trilinear diagram, however, provides a graphical representation of the main processes that intervene in a coastal aquifer with regards to seawater intrusion. These processes include the exchange reactions between major cations, and the presence of dominant ions which represent seawater and freshwater facies (Giménez-Forcada, 2010). Displaying major ion analysis results using HFE-D diagrams for different time periods (2007 vs. 2017) can provide useful insight into the varying extent of seawater intrusion into the Todos Santos Aquifer.

3.2 Groundwater Modeling

Groundwater flow models were constructed using data published in 2007 (CONAGUA, 2007), including well and surface water locations, pumping rates and durations, hydraulic head, and specific conductance, as well as data acquired from the June 2017 field investigation (Table 1). Models were created using SEAWAT, a numerical simulation code capable of simulating density-dependent groundwater flow problems, commonly used in seawater intrusion applications (Langevin et al., 2008). Three modeling simulations were constructed:

1) A transient model run until hydraulic heads and concentrations remained constant with time, calibrated to hydraulic head values and salinity values published in 2007,

2) A 10-year transient model calibrated to concentration values acquired in 2017, and

3) A group of forecasting models to analyze various recharge/discharge scenarios and their effect on seawater intrusion and aquifer sustainability, including scenarios simulating overexploitation of surface water resources, and simulations of sea-level rise. These models are hereto referred to as (1) Long-term Steady-State, (2) Transient (2007-2017), and (3) Forecasting Simulations.

This study utilized numerical modeling to analyze the extent of seawater intrusion into the Todos Santos Aquifer. The numerical model was constructed using SEAWAT-4000 (Langevin et al., 2008); Groundwater Vistas version 6 (Rumbaugh & Rumbaugh, 2011) was used as the graphical user interface in model development.

3.2.1 SEAWAT and Variable-Density Groundwater Flow

Investigations of groundwater flow in coastal aquifers can be more complicated because of spatial variations in fluid density (Langevin et al., 2008). Seawater intrusion is commonly modeled using SEAWAT, a variable-density groundwater flow model which couples flow and transport equations from USGS MODFLOW (Hill et al., 2000) and MT3DMS (Zheng and Wang, 1999) codes, allowing those familiar with the latter codes to simulate variable-density problems with relative ease. MODFLOW is a computer program that numerically solves the three-dimensional groundwater flow equation using the finite-difference method (Harbaugh et al., 2000). MT3DMS is a computer program that solves for modular three-dimensional solute transport in porous media, capable of simulating advection and dispersion processes applicable to seawater intrusion problems (Zheng and Wang, 1999). The variable-density groundwater flow equation utilized in SEAWAT is developed in terms of freshwater head and fluid density.

Fluid density varies from 1000 kg/m^3 for freshwater to 1025 kg/m^3 for seawater. This relatively minor variation in density has a substantial effect on groundwater flow rates and patterns (Guo & D.Langevin, 2002), and is therefore necessary to simulate when attempting to understand flow processes in coastal aquifers. SEAWAT is a modification of MODFLOW which uses equivalent freshwater head as the principal dependent variable, and conserves fluid mass rather than fluid volume (Guo & D.Langevin, 2002).

3.2.1.1 Mathematical Description of Variable-Density Groundwater Flow

SEAWAT is based on the concept of equivalent freshwater head in a saline groundwater environment (Guo & D.Langevin, 2002). This concept mathematically relates hydraulic heads of varying densities, such that the pressure head of saline water is converted to the resulting pressure head of purely freshwater, based on the differences in pressure caused by the differences in density. In depth explanation of this concept can be found in the SEAWAT User Manual, however, a brief description is explained here to facilitate understanding of the SEAWAT code.

Head in terms of aquifer water varies with pressure, elevation, and water density. This concept is demonstrated in Figure 5. Therefore, variations in water density will affect the resulting head measurement in the field as well as model calculation. Field measurements of hydraulic head in the aquifer and the corresponding equivalent freshwater head is related by the following relationship:

$$h_f = \frac{\rho}{\rho_f} h - \frac{\rho - \rho_f}{\rho_f} Z \qquad \text{(Equation 1)}$$

$$h = \frac{\rho_f}{\rho} h_f + \frac{\rho - \rho_f}{\rho} Z \qquad \text{(Equation 2)}$$

where:

h_f is the equivalent freshwater head [L],

h is the field-measured head [L],

ρ is the density of saline aquifer water [ML^{-3}],

ρ_f is the density of freshwater [ML^{-3}], and

Z is elevation of the water column [L].

Using this relationship simplifies the computational relationship between MODFLOW and SEAWAT codes.

The governing equation for variable-density groundwater flow is as follows:

$$-\nabla \cdot (\rho \vec{q}) + \bar{\rho} q_s = \rho S_p \frac{\partial P}{\partial t} + \theta \frac{\partial \rho}{\partial C} \frac{\partial C}{\partial t} \qquad \text{(Equation 3)}$$

where:

∇ is the gradient operator $\frac{\partial}{\partial x} + \frac{\partial}{\partial y} + \frac{\partial}{\partial z}$,

ρ is the fluid density [ML^{-3}],

$\vec{q}$ is the specific discharge vector [LT^{-1}],

$\bar{\rho}$ is the density of water entering from a source or leaving through a sink [ML^{-3}],

q_s is the volumetric flow rate per unit volume of aquifer representing sources and sinks [T^{-1}],

S_p is the specific storage in terms of pressure [$M^{-1}LT^2$],

θ is porosity [dimensionless],

t is time [T],

P is fluid pore pressure [$ML^{-1}T^{-2}$], and

C is solute concentration [ML^{-3}].

This equation is derived from the mathematical expression for conservation of mass and is described in detail in the User's Guide to SEAWAT (Guo & D.Langevin, 2002). The governing equation includes a term for specific discharge, which is calculated with Darcy's law. The general form of Darcy's law for a variable-density fluid is expressed by the equations:

$$q_x = -\frac{k_x}{\mu} \frac{\partial P}{\partial x} \qquad \text{(Equation 4)}$$

$$q_y = -\frac{k_y}{\mu}\frac{\partial P}{\partial y} \quad \text{(Equation 5)}$$

$$q_z = -\frac{k_z}{\mu}\left[\frac{\partial P}{\partial z} + \rho g\right] \quad \text{(Equation 6)}$$

where:

q_x, q_y, q_z are the individual components of specific discharge,
μ is the dynamic viscosity [$ML^{-1}T^{-1}$],
k_x, k_y, k_z represent intrinsic permeabilities [L^2] in the three coordinate directions, and
g is the gravitational constant [LT^{-2}] and is treated as a positive scalar quantity.
The governing equation for variable-density flow in terms of freshwater head as used in SEAWAT is as follows:

$$\frac{\partial}{\partial \alpha}\left(\rho K_{f\alpha}\left[\frac{\partial h_f}{\partial \alpha} + \frac{\rho - \rho_f}{\rho_f}\frac{\partial Z}{\partial \alpha}\right]\right) + \frac{\partial}{\partial \beta}\left(\rho K_{f\beta}\left[\frac{\partial h_f}{\partial \beta} + \frac{\rho - \rho_f}{\rho_f}\frac{\partial Z}{\partial \beta}\right]\right) + \frac{\partial}{\partial \gamma}\left(\rho K_{f\gamma}\left[\frac{\partial h_f}{\partial \alpha} + \frac{\rho - \rho_f}{\rho_f}\frac{\partial Z}{\partial \gamma}\right]\right) = \rho S_f \frac{\partial h_f}{\partial t} + \theta \frac{\partial \rho}{\partial C}\frac{\partial C}{\partial t} - \bar{\rho} q_s \quad \text{(Equation 7)}$$

where:

α, β, γ correspond to the coordinate axes aligned with permeability directions

K_f is the freshwater hydraulic conductivity [LT^{-1}], and

S_f if the specific storage in terms of freshwater head [L^{-1}].

The relationship between the density of saltwater and concentration is:

$$\rho = \rho_f + EC \quad \text{(Equation 8)}$$

$$\frac{\partial \rho}{\partial C} = E = 0.7143 \quad \text{(Equation 9)}$$

The SEAWAT code functions in two parts. Cell-by-cell flow is calculated from freshwater head gradients at the beginning of each flow time step, then the calculated flow field is passed to MT3DMS, where the density field is calculated from solute concentrations. The

resulting density field is then passed back to MODFLOW, where a new cell-by-cell flow is calculated for the following time step. In summary, all groundwater flow equations for constant-density simulations, as used in MODFLOW, are converted from solving for volumetric flux to solve for mass flux by replacing the pressure term with that of equivalent freshwater head (Guo & D.Langevin, 2002).

3.2.2 Model Design

Boundary conditions and model properties were assigned based on data published in CONAGUA's 2007 study of the Todos Santos Aquifer and surrounding aquifers. Models were discretized based on the scale of available digital elevation data (INEGI) and estimated well depths. Information published in CONAGUA's 2007 study which aided in model construction includes well locations, pumping rates, well operation times, static water levels and specific conductance values. Data published for surrounding aquifers aided in construction of model boundary conditions. Surrounding aquifer data was also used in interpolation to create initial parameter datasets for model input using ArcGIS.

An initial long-term steady-state SEAWAT model was constructed to calibrate hydraulic conductivity and recharge values to 12 hydraulic head values and 27 salinity values published in 2007. A second transient SEAWAT model was constructed to calibrate any unknown changes in pumping rates over the ten year span from 2007 to 2017 – this model was calibrated to relative concentrations in the form of salinities, converted from specific conductance data collected in 2017. Results from the transient 2007-2017 scenario were used as initial conditions for various forecasting scenarios.

3.2.3 Model Domain

The Todos Santos Aquifer boundary as delineated by CONAGUA (Figure 1) reaches nearly 27 km inland and measures 10 km wide along the coastline. For modeling purposes, the northeastern boundary was placed at around 10 km inland due to lack of far inland data, making the total active area 87.75 km^2. The lower aquifer boundary is modelled at 40 meters below sea level, based on estimated well depths. Well depth measurements were unavailable and were therefore estimated based on a cross-section published in CONAGUA's 2007 study (Figure 6). The remainder of well depths were extrapolated from those measured from Figure 6.

The model is 3-dimensional with six layers to simulate vertical concentration gradients near the coastline. The upper-most layer is variable in thickness due to the implemented digital elevation model, however, its lower boundary is modelled at 5 meters below sea level. The following three layers are each 5 meters in thickness, while the lower two are 10 meters in thickness. The model grid is 50 by 50 meters with 210,580 active cells.

3.2.4 Model Parameters

Recharge to the aquifer was simulated using injection wells on the northeastern aquifer boundary. Recharge rates of 120 mm/year have been published in previous government reports (Federman, 2015), however, Carmona (2017) published that estimated aquifer recharge was as little as 6 mm/year, with the remainder of precipitation being lost to surface runoff and evapotranspiration. Multiple recharge rates were simulated, with 6 mm/year being the final value used for all model scenarios. An injection rate of 0.98 m^3/d was applied over 1,962 cells between six layers comprising the northeastern aquifer boundary (Figure 8). This rate was calculated by multiplying the daily recharge rate by the upper watershed area (116,434,290.85 m^2) to obtain a volumetric recharge rate, then dividing that rate by the number of assigned injection cells to

obtain a volumetric injection rate per cell. A simulated injection rate of 0.98 m^3/d per cell assigned to 1,962 total cells results in a simulated recharge rate of 1,922.76 m^3/d. Two evapotranspiration zones were simulated using MODFLOW's Evapotranspiration Package (ET) (Harbaugh et al., 2000), one for palm trees and wetland areas near the coast, and another for inland agriculture fields. Areas of evapotranspiration were constructed based on the published Todos Santos vegetation map (INEGI). The wetland evapotranspiration was simulated as 0.001 m/d, while the agriculture field was simulated as 0.0018 m/d, both having extinction depths of 1 meter below land surface. These values were estimated based on values published in Food and Agriculture Organization Irrigation and Drainage Paper No. 56. Dispersivity values varied between different aquifer material zones, and were manually calibrated by trial and error approach during the long-term steady-state simulation. Porosities for igneous and metamorphic rock types are highly variable (Fetter, 2001), and were estimated to be lower than that of the alluvium for the purposes of this study. Dispersivity values were estimated from values published for a horizontal scale of 500-1000 meters, and a vertical scale of 50 meters (Gelhar et al., 1993). The resulting model values used are listed in Table 2.

The model incorporates four zones of hydraulic conductivity based on the three main types of aquifer material (Calera et al., 2001) and the La Poza estuary as a surface water body. The four materials include fractured igneous and metamorphic bedrock, polymict conglomerate, fine-to-coarse grained basin-fill sediments (referred to as alluvium), and the La Poza estuary. The range of transmissivity values published in CONAGUA's 2007 study, along with aquifer thickness estimates up to 40 m, were used to estimate a range of hydraulic conductivity values. Published transmissivity values for the valley extent (alluvium) range from 1.31 to 84.78×10^{-3} m^2/s (CONAGUA, 2007). Model conductivity estimates were made using the relationship T =

Kb, where *T* = Transmissivity, *K* = Hydraulic Conductivity, and *b* = aquifer thickness. For an aquifer thickness of 40 m, the range of conductivity values resulting from the presented transmissivity values (CONAGUA) were 2.8 to 183.12 m/d for the alluvium. Conductivity ranges for igneous/metamorphic bedrock and polymict conglomerate were estimated based on values published in Fetter (2001). The range of conductivity values were then manually calibrated by trial and error to accurately simulate groundwater flow according to the model domain. Wetlands can typically be simulated as high hydraulic conductivity nodes, (Anderson et al., 2015), therefore the La Poza estuary was assigned a hydraulic conductivity of 820 m/d, a value 100x the highest hydraulic conductivity value used in manual calibration efforts.

Initial concentration zones were created by performing inverse distance weighting analysis in ArcGIS on salinities converted from specific conductance data published by CONAGUA in 2007 (Table 3). A combined total of 70 samples from both Pescadero and Todos Santos Aquifers were used in the analysis. Values of salinity were used as concentration inputs to the SEAWAT model. Salinity is often close to the dissolved-solids concentration, however, must be converted into concentration units of mass per volume (Guo & D.Langevin, 2002). Specific conductance values were converted to salinity for use in SEAWAT using the following relationship for conversion from specific conductance to salinity at 25°C (Lewis, 1980):

$$S = K_1 + \left(K_2 * R^{\frac{1}{2}}\right) + (K_3 * R) + \left(K_4 * R^{\frac{3}{2}}\right) + (K_5 * R^2) + (K_6 * R^{\frac{5}{2}}) \qquad (10)$$

where:

K_1 = 0.0120
K_2 = -0.2174
K_3 = 25.3283
K_4 = 13.7714

K_5 = -6.4788

K_6 = 2.5842, and

R is the ratio of the sample specific conductance at 25°C to that of standard seawater (35 kg/m^3).

Inverse distance weighting analysis resulted in eight concentration zones, shown in Figure 9. A salinity value of 17.5 kg/m^3 was assigned to the La Poza estuary to represent mixing of seawater and freshwater, and a salinity value of 35 kg/m^3 was assigned to the constant head boundary representing the ocean.

Model properties, including initial concentration, hydraulic conductivity, dispersivity, porosity, and specific yield were simulated as constant with depth over the six model layers (with the exception of the zone simulating La Poza estuary, assigned to layer 1, exclusively). Evapotranspiration was applied to the top layer only.

3.2.5 Model Boundary Conditions

The coastline and the La Poza estuary were both assigned constant head boundaries, using MODFLOW's BAS6 Package (Harbaugh et al., 2000), at a value of 0 meters above mean sea-level. MODFLOW's General Head Boundary (GHB) Package (Harbaugh et al., 2000) was used to assign head-dependent flux boundaries to the northwest and southeast aquifer boundaries in order to simulate connection with the surrounding aquifers. The values assigned to these head-dependent boundary conditions were based on hydraulic head values published in CONAGUA's 2007 study for the Cañada Honda Aquifer to the northwest of Todos Santos and the Pescadero Aquifer to the southeast. The distance to GHB head was set at 500 m for both boundaries. GHB cells were assigned concentrations corresponding to their location within initial concentration zones (Figure 9). No-flow boundary cells were assigned to all area outside the delineated aquifer

area. The northeastern boundary was assigned injection wells using MODFLOW's Well package (Harbaugh et al., 2000) to simulate recharge from high topographic infiltration in the northeastern portion of the aquifer. Boundary conditions are displayed in Figure 8.

The main surface runoff, Arroyo La Reforma, was modeled using the MODFLOW River (RIV) package (Harbaugh et al., 2000). Water normally flows in Arroyo La Reforma year-round in the lower topographic region of Todos Santos, however it has recently been reported that surface flow no longer reaches the La Poza estuary as it once did. The RIV cells representing La Reforma were also utilized to simulate an additional area of isolated recharge within the stream channel. Eastoe et al. (2015) found that recharge to the aquifer is from large storm events, and originates in the lower elevations of the watershed (< 400 m) during runoff. Because Arroyo La Reforma runs through these lower elevations, RIV cells were used to simulate the additional recharge captured in the stream channel from large storm events. La Reforma was modeled as a steady-state boundary condition in all models. A water level of 1 meter above ground level was assumed throughout the stream. River-bed thickness was estimated to be 0.5 meters with a hydraulic conductivity of 2 m/day. RIV cells were assigned concentration values corresponding to their location within initial concentration zones (Figure 9). Stream width was measured in various segments using Google Earth, with an average of 5 meters being used in the model simulation.

In addition to simulating recharge, MODFLOW's Well package (Harbaugh et al., 2000) was used to model domestic wells, agricultural wells, and springs. A total of 23 wells were included in the model. Wells labelled as "Not in Use" in CONAGUA's publication were not included in well assignments, however, hydraulic head and specific conductance data collected from these sources were used in implementation of model targets. Pumping rates, durations, and

well depths in the form of model layer are listed in Table 4 were assigned to well locations in the steady-state model. Pumping rates were assigned to corresponding stress periods based on operation time. Well depth data was unavailable, and was therefore estimated based on the cross-section published in CONAGUA's 2007 study (Fig. 6). Well depths were measured from Figure 6, then the remainder of well depths were extrapolated based on these depths combined with assumed aquifer geometry by hand contouring, with coastal wells being assigned to layer 5 and the furthest inland wells being assigned to layer 1. Layer assignments for each well are listed in Table 4, with the deepest wells assigned to layer 5 at 30 meters below sea level.

3.3 Long-term Steady-State Simulation

Terminology regarding steady-state and transient scenarios can be confusing when referring to variable-density models due to the coupling of flow and transport components (Guo & D.Langevin, 2002). Flow is considered to be at steady-state when heads do not change with time, and transport is considered to be at steady-state when concentrations do not change with time. In this study, the steady-state model included initial concentrations and appropriate hydrologic stresses from the year 2007, and was run until both concentrations and heads became constant with time to represent the model reaching steady-state conditions. The purpose of running a steady-state simulation for a variable-density model is to allow concentrations and heads to equilibrate, creating a numerically stable initial condition input for transient simulations (Guo & D.Langevin, 2002). This study also utilized the long-term steady-state model in calibration of hydraulic conductivity values, recharge rates, and streambed conductance values.

The long-term steady-state scenario simulated roughly 75 years. A total of 150 stress periods were simulated, each at a length of 180 days.

3.4 Long-term Steady-State Model Performance and Calibration

The long-term steady-state model was performed to calibrate hydraulic conductivity values and streambed conductance values. These parameters were calibrated principally to measured hydraulic head values and secondarily to salinity values (converted from specific conductance values), both published in CONAGUA's 2007 study. A total of 14 hydraulic head targets and 27 concentration targets were used in calibration (Fig. 10). Target locations were assigned to layers corresponding to estimated well depths (Fig. 6). Calibration target locations and values are listed in Table 5. Calibration was done by a manual trial-and-error approach for each parameter.

Two calibration statistics were used to assess model performance: Division of the mean absolute error (MAE) over the range of observed values, and the scaled root mean square error (scaled RMSE). Both of these result in a percentage error value. A target error value of <10% was aimed for with respect to reproduction of hydraulic head values, and an error value of <20% was aimed for with respect to concentration values. Using concentration values for calibration in seawater intrusion models is considered difficult and subject to various discrepancies (Carrera et al., 2010), and therefore less emphasis was placed on accurately reproducing these values. Carrera et al. (2010), explains the various difficulties which arise in the inverse modeling of seawater intrusion, including the following: (1) Salinity concentration data are sensitive to flow within the borehole (worsened by pumping), (2) Salinity concentration measurements in open wells may not reflect resident aquifer concentrations but flux averaged concentrations – this is particularly significant in seawater intrusion problems, where vertical fluxes are likely to occur within the borehole, (3) Salinity is highly sensitive to heterogeneity in hydraulic conductivity and to the presence of preferential flow paths, and (4) Salinity is highly sensitive to aquifer

bathymetry. Unknown parameters in this study, including aquifer bathymetry, well depth, screen intervals, and pumping conditions during the time concentrations were measured in 2007, exacerbate the difficulty in calibrating to concentration values.

3.5 Transient (2007-2017) Simulations

Two transient scenarios were simulated for a time period of 10 years for the purpose of calibrating unknown pumping rates between the years 2007 and 2017. Pumping rates were calibrated to salinity values converted from specific conductance values collected in 2017 (Table 3). These simulations utilized stricter solver parameters (smaller head change criterion) and a smaller transport step size to provide a more accurate final solution, and consequently a more accurate initial condition to input into forecasting models. These simulations implemented a head change criterion of 0.001 m, as oppose to the head change criterion of 0.1 m used in the long-term steady-state simulation. Six time steps per stress period were simulated (flow was calculated once per month), while seven transport steps were simulated per flow step (concentration was calculated seven times per month, 42 times per stress period). These solver parameters remained the same for forecasting scenarios.

3.5.1 Transient (2007-2017) Model Design

Hydraulic head and concentration results from the long-term steady-state simulation were used as initial conditions for the transient simulation. A transport step size of 1 day and a step size multiplier of 1.5 was used, making a total of 7 transport steps for each groundwater flow time step. Stress periods were designed to be 180 days in length to represent growing and non-growing irrigation cycles, coinciding with growing and non-growing time periods for crops watered by agricultural wells. Twenty stress periods were used, totaling roughly 10 years. Recharge remained constant throughout the simulation at 6 mm/year. In the first scenario,

pumping rates remained equal to the rates published in 2007 (CONAGUA, 2007) (Table 4). Because Todos Santos has experienced population growth from 2007 to 2017 (INEGI), pumping rates for irrigation wells and for wells near the coast were increased by 100% (Table 4). Results from both simulations were compared to analyze which pumping rates more accurately reproduced concentration data collected in 2017, as hydraulic head data were unavailable. Results from the transient scenario (hydraulic heads, concentrations) were used as initial conditions for various forecasting scenarios.

3.6 Forecasting Simulations

Various forecasting scenarios were modelled, with changes made to pumping rates, recharge rates, and surface water sources. The objective of forecasting was to reasonably predict the extent of seawater intrusion into the aquifer as a consequence of population growth and increased development. Time periods of five, ten, and twenty years were simulated for each pumping scenario. For one scenario, pumping rates remained equal to those calibrated in the transient scenario (Table 4). A second scenario simulated increased pumping by 100% of published 2007 values in all wells (Table 4). A third scenario analyzed the effect of sea-level rise at a rate of 4 mm/yr, close to the average global rate of sea-level rise according to NASA (NASA, 2018). A fourth scenario implemented overexploitations of the lower reaches of Arroyo La Reforma to analyze the impact of surface water on the extent of seawater intrusion. There is evidence in the form of anecdotal reports by locals, as well as historical imagery from Google Earth, that Arroyo La Reforma has already been overexploited in lower reaches of the stream, which previously provided flow into La Poza estuary (Fig. 11). Simulating this effect was done by manually deleting RIV cells for ten and twenty year forecasting simulations, corresponding to the lower 500 m and 750 m of Arroyo La Reforma, respectively. The fifth scenario analyzed the

effect of severe sea-level rise at a rate of 25 mm/yr. The extent of seawater intrusion was analyzed for two coastal areas of the aquifer: (1) The area in close proximity to Arroyo La Reforma and the town of Todos Santos, and (2) Punta Lobos beach, the location of recent development (Fig. 7).

Easting coordinates of the seawater-freshwater interface were identified and plotted at depth along cross-sections corresponding to areas (1) and (2). The evolution of the seawater-freshwater interface for each layer was calculated for five, ten, and twenty years following 2017. This evolution was calculated in terms of distance from the 2017 simulated interface, as well as distance from the coastline. Layer 5 is chosen to represent plan-view concentration contours due to this depth's increased susceptibility to the effects of seawater intrusion, as it contains the most pumping wells closest to the coastline.

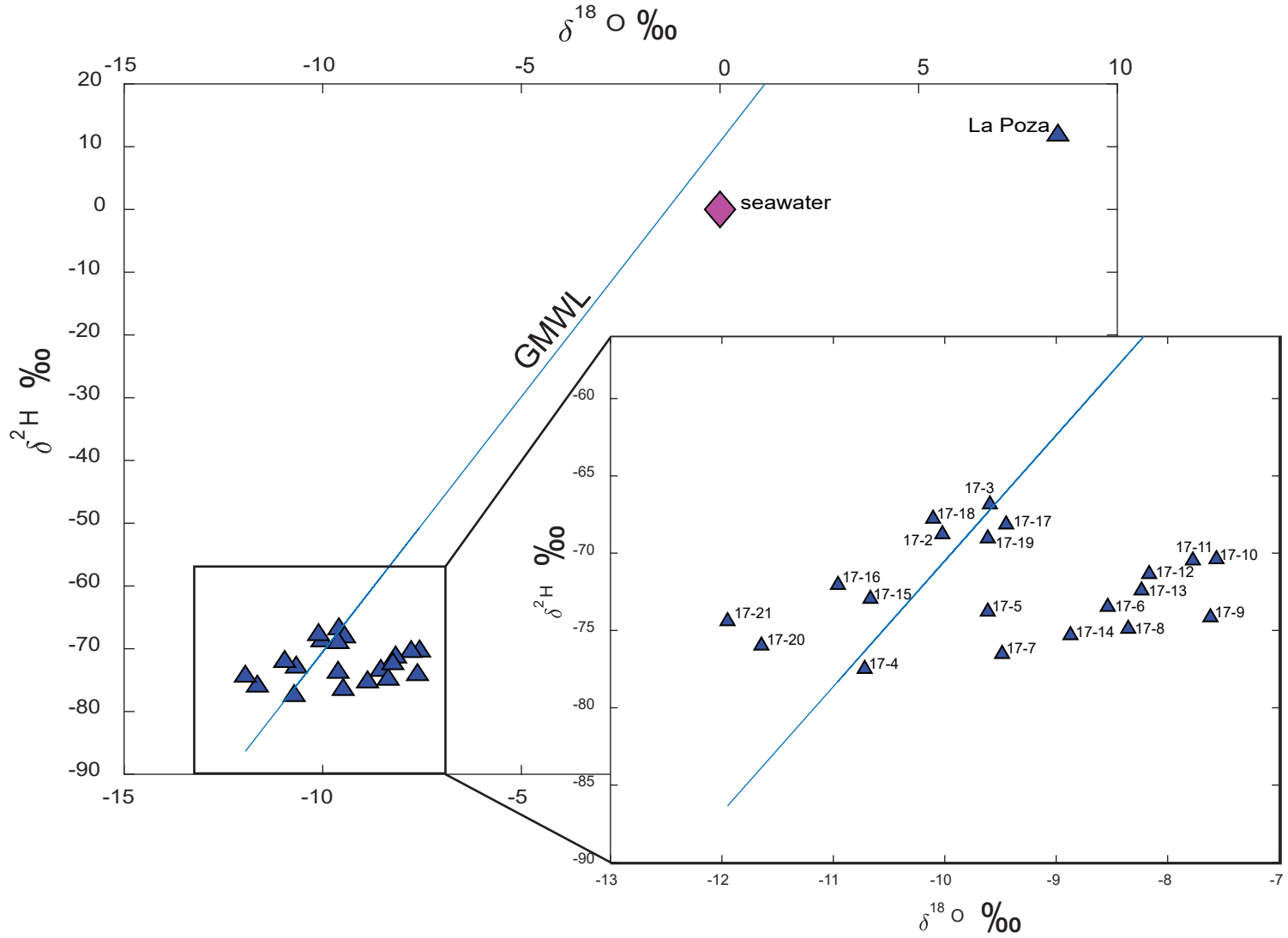

Figure 4: Stable isotope analysis results from June 2017 field investigation. Isotopic signatures are generally depleted, indicating that groundwater recharge is sourced from hurricane precipitation (Eastoe et al., 2015). Samples plotting to the right of the Global Meteoric Water Line (GMWL) indicate groundwater which has been subject to evaporation. The location of the sample taken from La Poza relative to seawater indicates that its composition is that of evaporated seawater, suggesting a lack of freshwater influx.

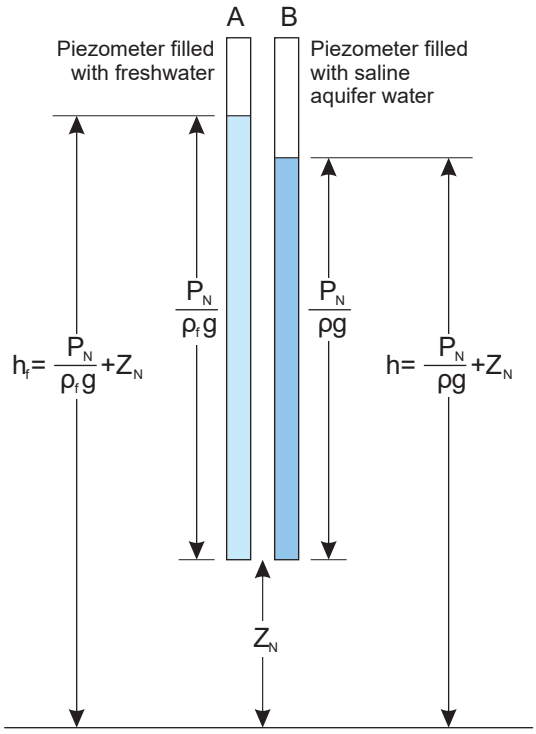

EXPLANATION

h_f	Equivalent freshwater head [L]
h	Head [L]
P_N	Pressure [$ML^{-1}T^{-2}$]
ρ_f	Density of freshwater [ML^{-3}]
ρ	Density of saline aquifer water [ML^{-3}]
g	Acceleration due to gravity [LT^{-2}]
Z_N	Elevation [L]

Figure 5: Two piezometers, one filled with freshwater and the other filled with saline aquifer water, open to the same point in the aquifer. From Guo and D. Langevin, 2002.

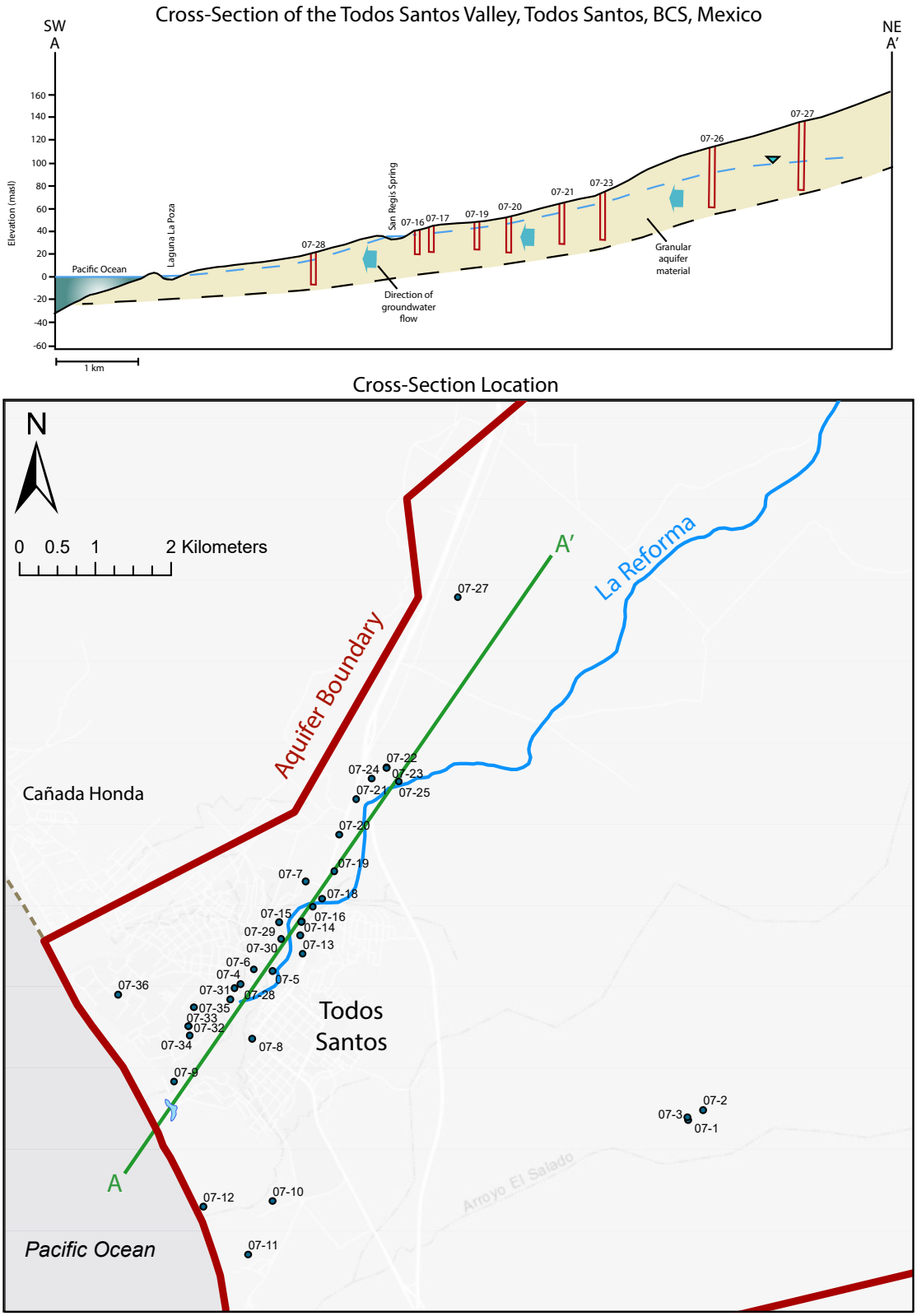

Figure 6: Cross-section of the Todos Santos Aquifer within the Todos Santos Valley, modified from CONAGUA (2007). Well depths were estimated based on the above cross-section, as well depth data was unavailable. Generally, wells reaching greatest depths are located near the coastline, and get progressively shallower with distance inland.

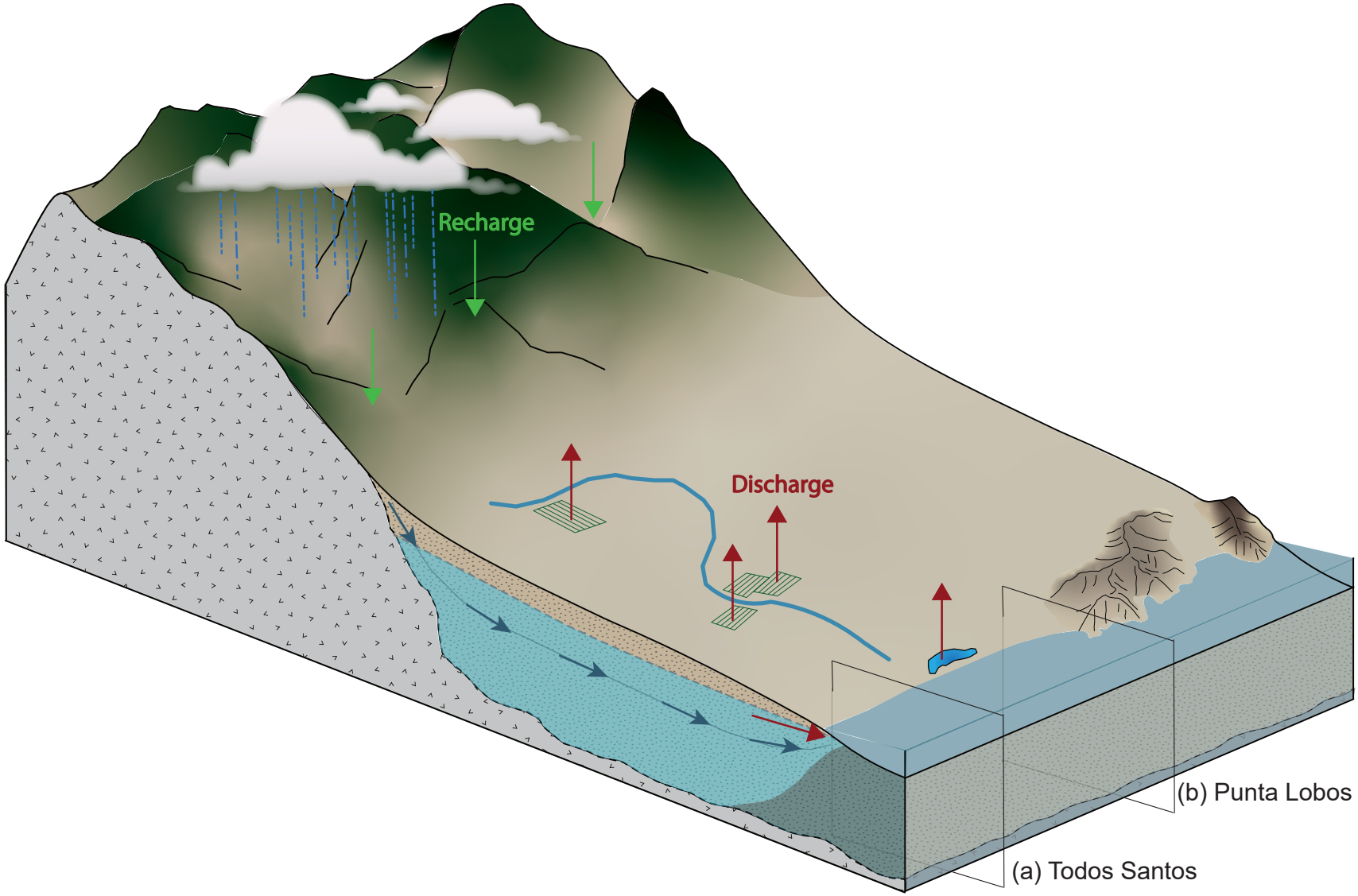

Figure 7: Conceptual model of the Todos Santos Aquifer (not to scale). Locations of seawater intrusion analysis from numerical simulation results are shown in panels (a) and (b). Location (a) is the area of the Todos Santos town in close proximity to Arroyo La Reforma. Location (b) is Punta Lobos beach, an area experiencing recent hotel development, and includes a water well located close to the coastl ine.

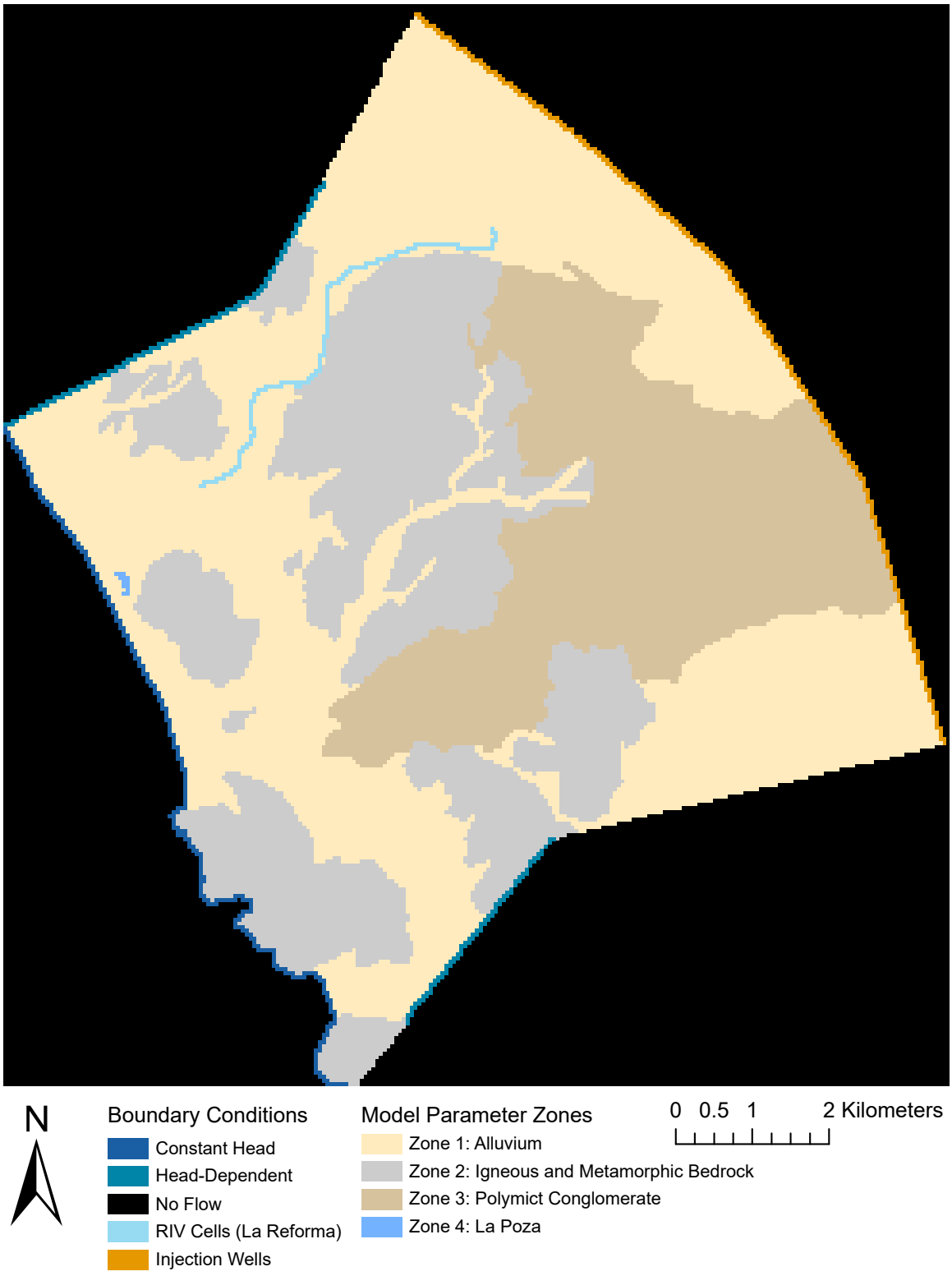

Figure 8: Boundary conditions and model parameters for SEAWAT model setup. Parameter zones are constructed based on the geologic map of the area (Calera et al. 2001). Aquifer connection with the Pacific Ocean is simulated with constant head cells, connection with surrounding aquifers is simulated with head-dependent flux cells, Arroyo La Reforma is simulated with RIV cells, and aquifer recharge is simulated by injection wells on the northeast boundary.

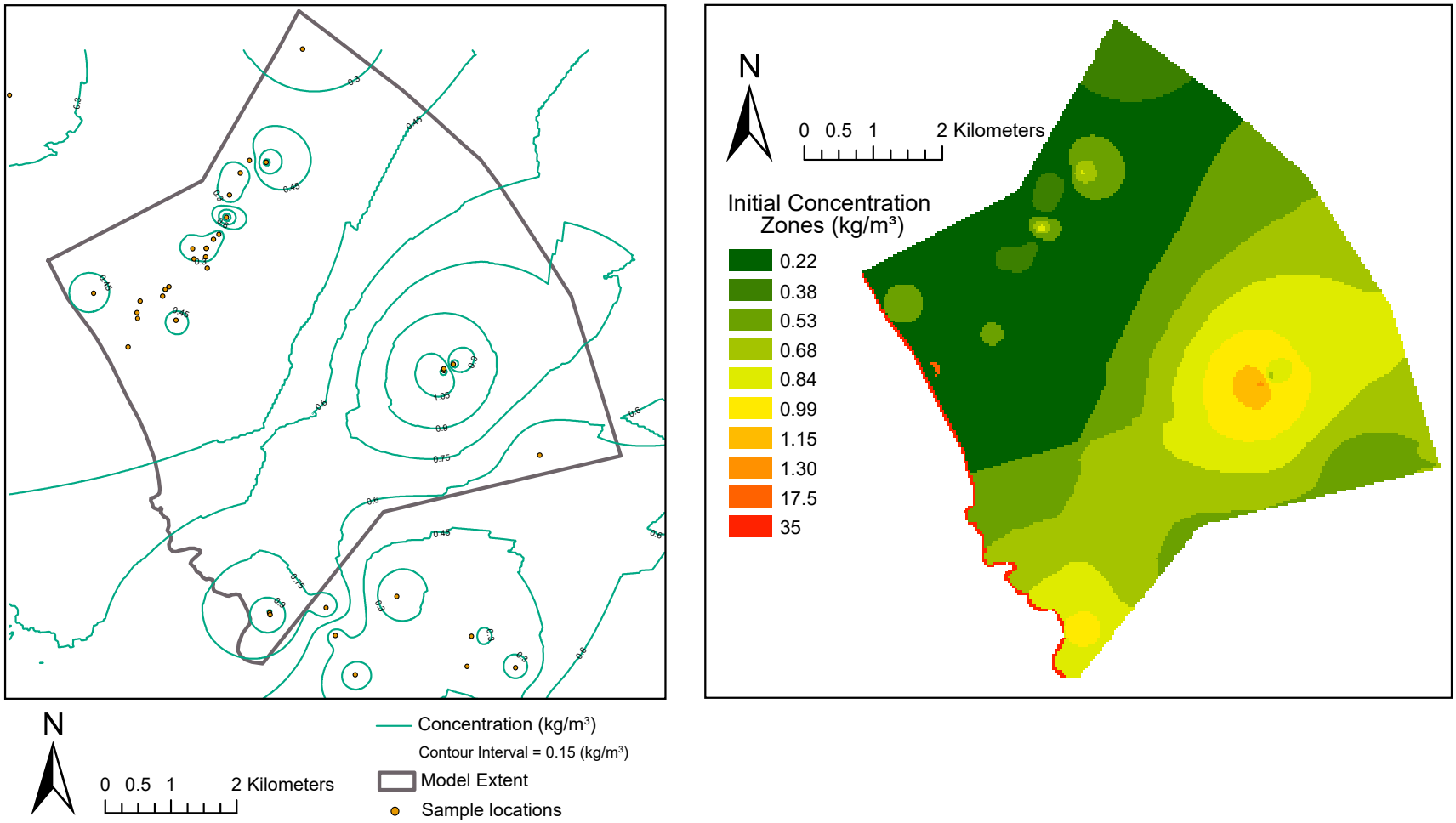

Figure 9: Construction of initial salinity zones for input into steady-state SEAWAT model. Figure 8(a) displays the results of inverse distance weighting analysis done on 70 salinity values encompassing Todos Santos, Pescadero, and Canada Honda Aquifers, and 8(b) displays the initial salinity zones constructed from the results shown in 8(a).

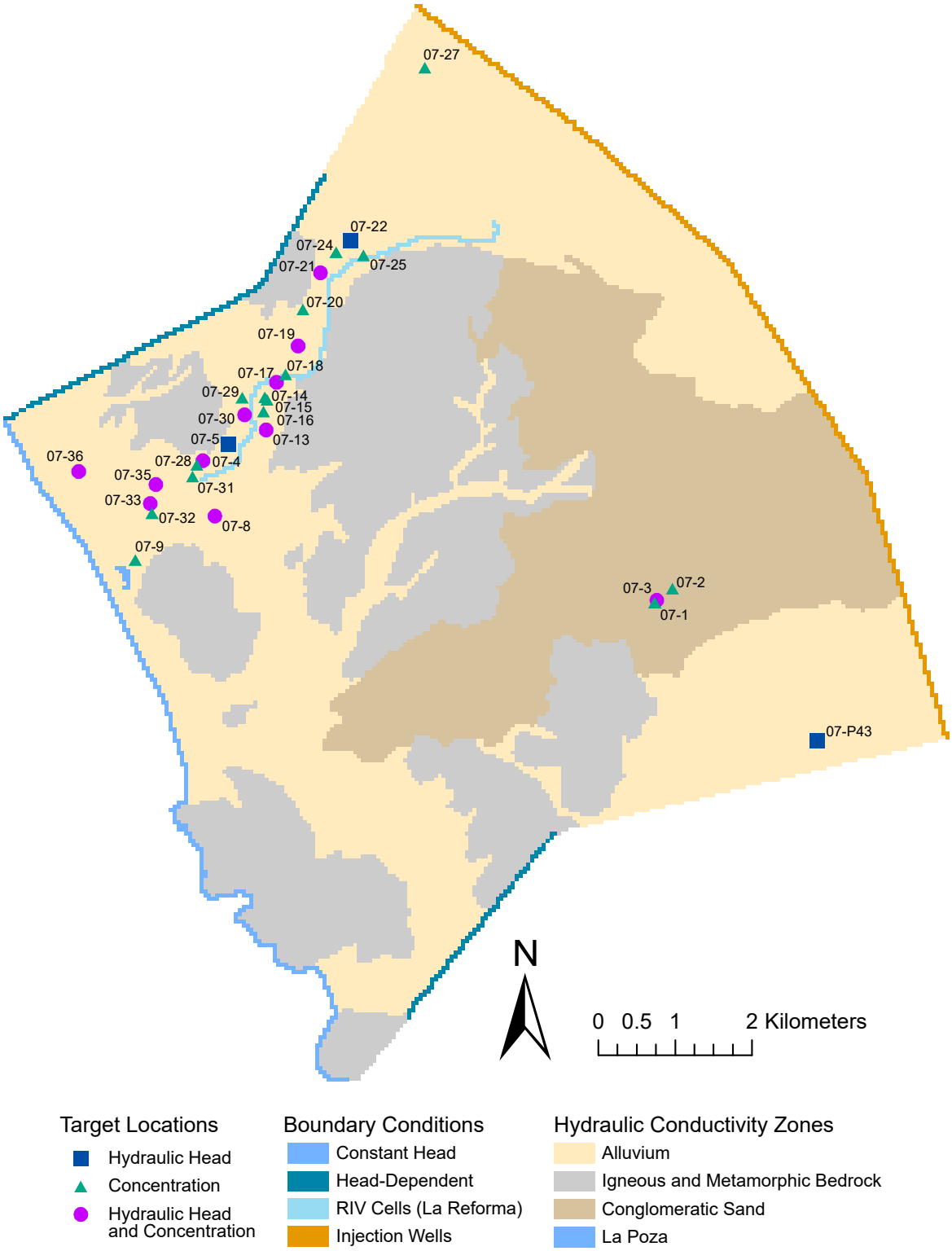

Figure 10: Steady-state model target locations and display of target types (hydraulic head and salinity) utilized in calibration. Data was compiled from CONAGUA (2007).

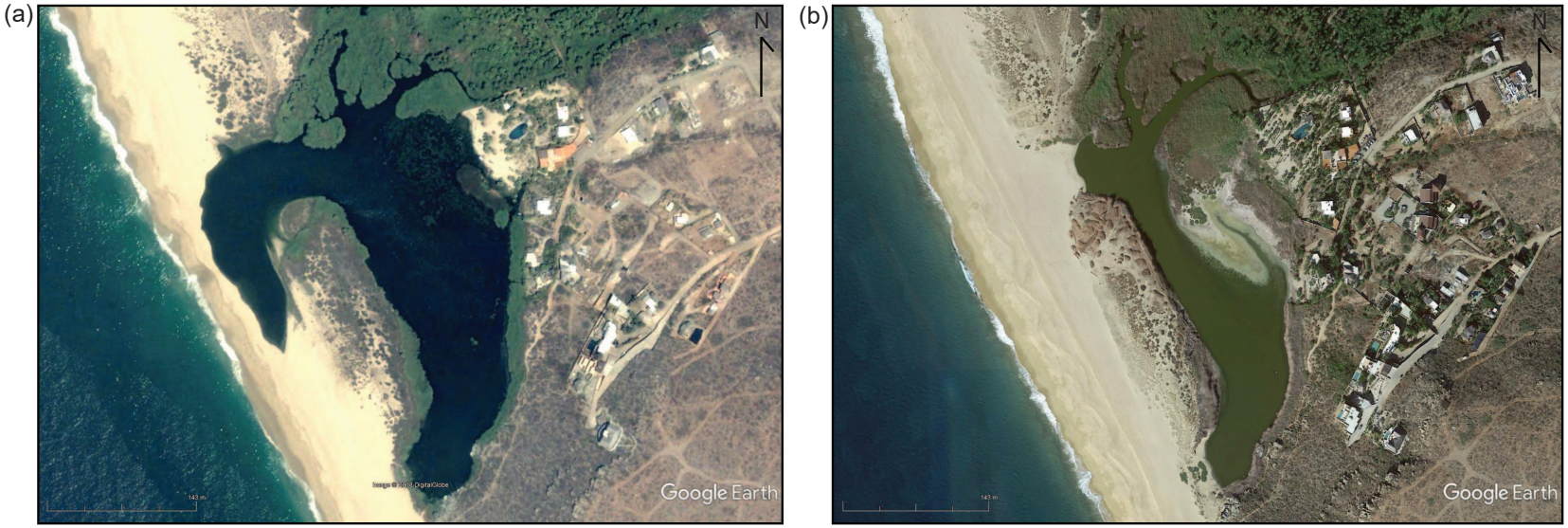

Figure 11: La Poza estuary in (a) August of 2007 and (b) December of 2016. Precipitation records show that Todos Santos received a total of 188.5 mm of rain in 2006 and 226.6 mm of rain in 2007, both values being above average (150 mm/yr) for the area (Tres Santos, 2012). A noticeably drier estuary can be seen in (b), as well as an increase in housing and development in the immediate surrounding. La Poza's isotopic signature in 2017 is indicative of evaporated seawater (Fig. 4), suggesting a lack of freshwater influx necessary for habitat diversity (Carrera et al., 2017).

Table 2: Calibrated model parameters from steady-state SEAWAT simulation

Zone No.	Material	Porosity	Specific Yield	Longitudinal Dispersivity (m)	Horizontal Transverse Dispersivity (m)	Vertical Transverse Dispersivity (m)	Hydraulic Conductivity (m/d)
1	Alluvium	0.25	0.1	100	10	0.005	5
2	Igneous and Metamorphic Basement	0.1	0.05	20	5	0.0008	0.0146
3	Polymict Conglomerate	0.2	0.1	100	10	0.005	2
4	La Poza Estuary	1.0	0.5	100	10	0.005	820

Table 3: Salinity values, converted from collected specific conductance values, for 2007 and 2017. 2007 salinity values were used in steady-state model calibration. 2017 salinity values were used in calibrating the first transient model, simulating the 10 year time span from 2007 to 2017.

2007	
Sample	**Salinity (kg/m^3)**
07-1	1.27
07-2	0.66
07-3	1.17
07-4	0.35
07-8	0.51
07-9	0.35
07-13	0.32
07-14	0.29
07-15	0.29
07-16	0.29
07-17	0.28
07-18	0.27
07-19	0.83
07-20	0.19
07-21	0.16
07-24	0.39
07-25	0.78
07-26	0.18
07-27	0.15
07-28	0.47
07-29	0.25
07-30	0.30
07-31	0.38
07-32	0.37
07-33	0.43
07-35	0.43
07-36	0.51

2017	
Sample	**Salinity (kg/m^3)**
17-1	51.41
17-2	0.65
17-3	0.44
17-4	0.22
17-5	0.19
17-6	0.22
17-7	0.21
17-8	0.29
17-9	0.57
17-10	0.68
17-11	0.60
17-12	1.29
17-13	0.66
17-14	0.36
17-15	0.59
17-16	0.45
17-17	0.53
17-18	0.60
17-19	0.80
17-20	2.56
17-21	0.46

Table 4: Pumping rates, pumping durations, and assigned model layer for wells published by CONAGUA (2007). Pumping rates are listed for different model scenarios.

Well No.	Use	Location		Operation Time		Steady-State	Transient final (2007-2017)	Forecast Scenario 1	Forecast Scenario 2	Forecast Scenario 3	Forecast Scenario 4, 5	Assigned Model Layer
		Northing (m)	Easting (m)	(hrs/day)	(days/yr)	Q (m^3/d)	Q (m^3/d)					
07-1	Domestic	2592040	584642	0.5	365	1.8	1.8	1.8	3.6	1.8	1.8	1
07-5	Potable	2594011	579159	12	365	1555.2	1555.2	1555.2	3110.4	1555.2	1555.2	4
07-6	Potable	2594027	578913	10	365	432	432	432	864	432	432	4
07-7	Domestic	2595193	579595	10	365	576	576	576	1152	576	576	2
07-8	Domestic	2593116	578891	2	365	28.8	57.6	57.6	57.6	57.6	57.6	5
07-13	Domestic and Agriculture	2594235	579557	4	180	28.8	57.6	57.6	57.6	57.6	57.6	4
07-14	Agriculture	2594478	579524	20	26	166.4	332.8	332.8	332.8	332.8	332.8	4
07-16	Domestic and Agriculture	2594660	579538	8	180	57.6	115.2	115.2	115.2	115.2	115.2	3
07-17	Domestic and Agriculture	2594855	579693	4	180	57.6	115.2	115.2	115.2	115.2	115.2	2
07-18	Canal	2594962	579812	24	365	10368	10368	10368	20736	10368	10368	2
07-19	Domestic and Agriculture	2595326	579974	3	26	97.2	194.4	194.4	194.4	194.4	194.4	2
07-20	Domestic and Agriculture	2595807	580037	20	180	2880	5760	5760	5760	5760	5760	2
07-21	Agriculture	2596279	580265	24	180	4320	8640	8640	8640	8640	8640	1
07-22	Agriculture	2596697	580662	12	180	3456	6912	6912	6912	6912	6912	1
07-27	Agriculture	2598939	581603	18	180	2332.8	4665.6	4665.6	4665.6	4665.6	4665.6	1
07-28	Industrial	2593784	578658	4	180	129.6	259.2	259.2	259.2	259.2	259.2	5
07-29	Canal	2594655	579247	24	365	12096	12096	12096	24192	12096	12096	4
07-30	Canal	2594432	579276	24	365	12096	12096	12096	24192	12096	12096	4
07-31	Canal	2593635	578602	12	365	4320	8640	8640	8640	8640	8640	5
07-32	Agriculture	2593157	578070	8	180	115.2	230.4	230.4	230.4	230.4	230.4	5
07-33	Agriculture	2593279	578050	4	180	230.4	460.8	460.8	460.8	460.8	460.8	5
07-35	Domestic and Agriculture	2593528	578120	6	180	194.4	388.8	388.8	388.8	388.8	388.8	5
07-36	Domestic and Agriculture	2593697	577123	3	180	97.2	194.4	194.4	194.4	194.4	194.4	5

Table 5: Steady-state calibration target locations and values.

Sample No.	Coordinates		Hydraulic Head (m amsl)	Salinity (kg/m^3)	Assigned Layer
	Easting (m)	Northing (m)			
07-1	584642	2592040	107.36	1.27	1
07-2	584841	2592175	-	0.66	1
07-3	584634	2592079	-	1.17	1
07-4	578736	2593836	15.97	0.35	5
07-5	579159	2594011	21.037	-	4
07-8	578891	2593116	6.998	0.51	5
07-9	577859	2592546	-	0.35	5
07-13	579557	2594235	27.749	0.32	4
07-14	579524	2594478	-	0.29	4
07-15	579543	2594663	-	0.29	4
07-16	579538	2594660	-	0.29	3
07-17	579693	2594855	40.082	0.28	2
07-18	579812	2594962	-	0.27	2
07-19	579974	2595326	58.974	0.83	2
07-20	580037	2595807	-	0.19	2
07-21	580265	2596279	61.604	0.16	1
07-22	580662	2596697	71.418	-	1
07-24	580468	2596547	-	0.39	1
07-25	580824	2596507	-	0.78	1
07-26	575320	2597948	-	0.18	5
07-27	581603	2598939	-	0.15	1
07-28	578658	2593784	-	0.47	5
07-29	579247	2594655	-	0.25	4
07-30	579276	2594432	27.014	0.30	4
07-31	578602	2593635	-	0.38	5
07-32	578070	2593157	-	0.37	5
07-33	578050	2593279	6.088	0.43	5
07-35	578120	2593528	6.81	0.43	5
07-36	577123	2593697	-3	0.51	5
P-43	586726	2590198	114.11	-	1

CHAPTER 4

RESULTS

4.1 Stable Isotopes

Stable isotope analysis results are shown in Figure 4. Stable isotope analysis shows $\delta^{18}O$ and $\delta^{2}H$ values that vary from approximately -12 to -6‰ and -77 to -67‰, respectively. This range of isotopic signatures is relatively depleted compared to values typical of this latitude (Eastoe et al., 2015).

4.2 Water Quality

Analysis of specific conductance values along with major ion analysis was used to evaluate spatial and temporal changes in water quality over the 10-year period between the years 2007 and 2017. In temporal analysis, although well locations differ from 2007 to 2017, 89% of 2007 samples and 90% of 2017 samples reside within the Todos Santos valley (Figures 2, 3). Comparisons are made with the goal of examining changes in the aquifer system as a whole, rather than for specific well locations.

4.2.1 Specific Conductance

Specific conductance data collected in 2017 (Table 1) was compared with the published data from 2007 (Table 1) with the intent to evaluate spatial and temporal changes in water quality. Sample locations and corresponding specific conductance values concentrated near the coast and around La Reforma are displayed in Figure 12 for years 2007 and 2017. Average, minimum, and maximum measured specific conductance values are summarized in Table 6. Mean specific conductance measured in 2007 was 888 µS/cm (microSiemens/centimeter) for 22

samples, with a minimum value of 308 µS/cm (Sample 07-27, located furthest inland) and a maximum value of 2,462 µS/cm (Table 6). Sample 07-1, corresponding to the maximum specific conductance value, is located outside the Todos Santos Valley extent, and has an anomalously high value, along with surrounding wells 07-2 and 07-3. The groundwater sample corresponding to the maximum specific conductance within the Todos Santos Valley extent is Sample 07-19. Other wells of notably high values (> 1,000 µS/cm) include Samples 07-8, 07-25 and 07-36. Mean specific conductance measured in June of 2017 was 1,210 µS/cm for 18 samples, with a minimum value of 390.9 µS/cm and a maximum value of 4,786 µS/cm (Table 6). The groundwater sample corresponding to the minimum specific conductance value (390.9 µS/cm), Sample 17-5, is located furthest inland, while the groundwater sample corresponding to the maximum specific conductance value (4,786 µS/cm), Sample 17-20, is located nearest the coast at Punta Lobos beach (Fig. 3).

4.2.2 Water Chemistry

Results of major ion analysis performed in 2007 and 2017 (Table 1) are displayed in Piper trilinear diagrams (Fig. 13) and hydrochemical facies evolution diagrams (HFE-D) (Giménez-Forcada, 2010) (Fig. 14). Hydrochemical and major ion facies outlined in Figure 13 are classified according to delineations by Back et al. (1966). Table 7 outlines the percentage of samples which fall into each category, calculated separately for water type, cation, and anion ternary diagrams (Fig. 13).

The majority of samples in both years fell into the mixed-type category (Fig. 13). A notable increase in chloride-type samples can be seen from 2007 to 2017, corresponding to 16.6% and 66.7%, respectively (Fig. 13) (Table 7). This increase is also evident in the sodium-chloride type category (Fig. 13), corresponding to 16.6% of 2007 samples and 19% of 2017

samples (Table 7). Samples classified as magnesium-bicarbonate type in 2017 correspond to wells located furthest inland, whereas samples classified as sodium-chloride type from the same time period correspond to wells located nearest the coastline (Fig. 13).

Samples from both time periods were also plotted on a hydrochemical facies evolution diagram (HFE-D) (Fig. 14) to analyze the saline status of the aquifer in terms of advancement/regression of the seawater-freshwater interface (Giménez-Forcada, 2010). Direct and inverse exchange reactions between cations are indicative of evolution between freshwater and seawater facies, and henceforth are used to analyze the state of intrusion in the Todos Santos aquifer during 2007 and 2017.

Samples were plotted on a HFE-D for 2007 (Fig. 14a) and 2017 (Fig. 14b). Year 2007 samples plotted 50% in the freshening phase and 50% in the intrusion phase. The location of the freshening-classified samples within the graph indicates late stage mixing, meaning the water is near equilibrium with the dominant flow (Giménez-Forcada, 2010). The plotted location of the intrusion-classified samples indicates both early and late stage mixing. 95% of year 2017 samples plotted in the intrusion phase (Fig. 14b), varying from early to late stage mixing. 47% of these samples plot in the NaCl and CaCl mix types. Notably, three samples are classified as NaCl-dominant, corresponding to the La Poza estuary and Las Palmas wetlands (surface water sources), and TS-20 (Punta Lobos, groundwater), defined as an evolution toward the seawater facies (Giménez-Forcada, 2010). Wells geographically located furthest inland (17-4, 17-5, 17-6, and 17-7) correspond to samples plotting in the early stages of intrusion and in the freshwater facies, whereas samples from water sources geographically located closest to the coastline (17-1, 17-19, 17-20) correspond to samples plotting in the late stages of intrusion and in the seawater facies.

4.3 Groundwater Modeling

4.3.1 Long-term Steady-State

The long-term steady-state SEAWAT simulation, run for 75 years, was calibrated to 2007 hydrologic conditions and stresses. Pumping rates were assigned for growing and non-growing seasons, and therefore stresses varied between two 6 month periods within each year. Three zones of hydraulic conductivity were calibrated (alluvium, polymict conglomerate, igneous/metamorphic bedrock) to hydraulic head data. The same three zones were assigned dispersivity values, calibrated to salinity data. Layer 5 is chosen to represent salinity contours due to this depth's increased susceptibility to the effects of seawater intrusion, as it contains the most pumping wells closest to the coastline.

4.3.1.1 Long-term Steady-State Calibration Results

Long-term steady-state model parameters and boundary conditions were calibrated to 2007 hydrologic conditions and stresses. Calibration targets included hydraulic head and concentration values from CONAGUA's 2007 study (Table 5).

In terms of reproducing hydraulic head values, the long-term steady-state model produced a MAE/range value of 7.6% and a scaled RMSE of 12.7% (Table 8). Figure 15 shows simulated vs. observed head values for target locations. Two target values assigned to Layer 1 were vastly underestimated by the model, explaining a largely negative mean error of -6.4 m. These targets correspond to wells TS-1 and P-43, and are located in the southeastern quadrant of the aquifer. Data in this area is sparse and therefore reproduction of these values was challenging. Overall, a good fit of hydraulic heads in the area of interest was achieved.

In terms of reproducing concentration values, the steady-state model produced a MAE/range value of 11.6% and a scaled RMSE of 16.3% (Table 8). A mean error of -0.03 kg/m^3

was achieved, indicating little bias by the simulation. Simulated vs. observed salinity values are shown in Figure 16.

Model parameters calibrated to head and concentration values included hydraulic conductivities of three distinct geologic zones, streambed conductance, and dispersivity. Resulting hydraulic conductivities include 5 m/d for alluvium, 0.0146 m/d for igneous and metamorphic basement rock, and 2 m/d for polymict conglomerate (Table 2).

4.3.1.2 Long-term Steady-State Mass Balance

Figure 17 shows boundary conditions and corresponding contribution to the aquifer system for growing and non-growing seasons. Results are summarized in Table 9. RIV cells contribute most water to the system, while the surrounding pumping wells remove roughly the same amount. Discharge into the ocean boundary, comprised of constant head cells, is simulated to be 3.4 Mm^3/year, or around 107 liters per second. Water taken from storage is simulated to be 1,878 m^3/d during the growing season and 63 m^3/d during the non-growing season. Along with hydraulic heads and concentrations not changing with time, water taken from storage approaching 0 m^3/d is indicative that steady-state conditions were reached (Anderson et al., 2015).

4.3.1.3 Long-term Steady-State Water Table Contour Map

Steady-state simulated water table elevation is shown in Figure 18. Groundwater flow is from northeast to southwest, consistent with topographic driven flow from the Sierra de la Laguna Mountains.

4.3.1.4 Long-term Steady-State Concentration Contour Map

Figure 19 shows contoured salinity results for Layer 5 of the steady-state simulation. A high salinity gradient can be seen near the coast. The seawater-freshwater interface, identified at

contour 1.0 kg/m^3, is located at an average of 268 meters inland of the coastline, however reaches up to 607 meters inland.

4.3.2 Transient (2007-2017)

Three transient models were run over a 10-year timespan from 2007 conditions to 2017 conditions to calibrate unknown changes in pumping rates. Pumping rates and durations published in 2007 were used for the first simulation (no changes made from the long-term steady-state simulation). For the second simulation, pumping rates were doubled in coastal and irrigation wells, corresponding to population growth over the ten year period. The third scenario simulated pumping rates and durations published in 2007 along with sea-level rise of 4 mm/yr (NASA). Any potential changes in pumping rates from 2007 to 2017 were calibrated to 2017 concentration values.

4.3.2.1 Transient (2007-2017) Calibration Results

Statistically, the three transient simulations produced nearly identical values in terms of reproducing the observed 2017 concentration values, and the differences in error between the three scenarios was negligible (< 0.1%). Observed vs. simulated values of concentration are plotted in Figure 20.

In terms of reproducing 2017 concentration values, the 10-year transient simulation produced a MAE/range value of 9.4% and a scaled RMSE of 11.8% (Table 10). A mean error of -0.14 kg/m^3 was achieved, indicating the model is slightly biased in under-predicting concentration values. Most of this bias can be seen in wells closest to the coastline in Layer 5 (Figure 20). The mean simulated concentration of 0.47 kg/m^3 falls well within the first standard deviation of the mean observed concentration of 0.61 kg/m^3.

4.3.2.2 Transient (2007-2017) Mass Balance

The mass balance summary for the final time step in growing and non-growing periods is shown in Figure 21 and summarized in Table 11. The amount of water taken from storage varies from approximately 3600 m^3/d during growing season to 70 m^3/d during non-growing season. Over the course of one year, this amounts to approximately 660,000 m^3. Groundwater is provided principally by RIV cells in both seasons, with simulated inflow to the aquifer being 62,109 m^3/d and 48,049 m^3/d, respectively. Groundwater is extracted from the aquifer principally by wells, amounting to 69,859 m^3/d in the growing season and 41,503 m^3/d in the non-growing season. Simulated discharge into the ocean is around 9,000 m^3/d for both seasons, or approximately 104 liters per second.

4.3.3 Forecasting Simulations

4.3.3.1 Overview

Various forecasting scenarios were simulated to examine the extent of seawater intrusion, and the migration of the seawater-freshwater interface with time. To analyze the extent of seawater intrusion, the location of the seawater-freshwater interface was identified and plotted at depth for two different cross-section locations in the aquifer. Cross-section locations are shown in Figure 22. Plan-views of the simulated seawater-freshwater interface (identified at a salinity values of 1.0 kg/m^3) for years 2007 and 2037, model layer 5, are displayed in Figure 23 for each scenario. The location of these contours within the study area are shown in Figure 22 surrounding area (a) Todos Santos and (b) Punta Lobos. The cross-section locations analyzed are also shown in Figure 22. Layer 5 was chosen to represent salinity contours because of its increased risk of experiencing seawater intrusion, due to most of the pumping wells being located in that layer close to the coastline. Layer 1 was chosen to represent scenario 4, as that is

the layer where seawater intrusion was most affected by the corresponding changes in hydrologic stresses. Each plot includes the simulated seawater-freshwater interface location at the years 2007, 2017, 2022, 2027, and 2037. Seawater-freshwater interfaces are typically defined by a mixing zone. Water containing salt concentration over 1.0 kg/m^3 is considered saline (USGS, 2016), therefore the 1.0 kg/m^3 contour was defined as the interface location in this study for display purposes. Seawater-freshwater interface migration results are summarized in Table 12.

4.3.3.2 Scenario 1: Pumping rates remain at 2017 conditions

No alterations were made to model parameters for the first forecasting scenario. The resulting extent of seawater intrusion is shown in Figure 23. Between the years of 2017 and 2037, in the area of Todos Santos, the seawater-freshwater interface migrated an average of 0.7 meters inland with depth, putting the location of the interface at roughly 473 meters from the coastline (in comparison to a simulated interface location at roughly 464 meters from the coastline in 2007). Punta Lobos experienced an average seawater-freshwater interface migration of 30 meters inland, resulting in the interface location at 455 meters from the coastline.

4.3.3.3 Scenario 2: Pumping is doubled in all wells

In the second forecasting scenario, pumping was doubled in all pumping wells to simulate population growth and increased water demand. Extraction rates were not doubled in surface water sources (springs, canals). Between the years 2017 and 2037, the seawater-freshwater interface in the area of Todos Santos migrated an average of 1.29 m inland. The resulting interface location was simulated at 474 meters from the coastline. Punta Lobos experienced an average interface migration of 29.63 meters inland, resulting in an interface location approximately 455 meters from coastline.

4.3.3.4 Scenario 3: Pumping remains at 2017 conditions, sea-level rise of 4 mm/yr

With the addition of sea-level rise at an average rate of 4 mm/yr, the seawater-freshwater interface migrated an average of 1.57 meters inland in the area of Todos Santos between the years 2017 and 2037. The resulting interface location was simulated at 474 meters from the coastline. In the area of Punta Lobos, the interface migrated approximately 29.95 meters between the years 2017 and 2037, resulting in a location roughly 455 meters from the coastline.

4.3.3.5 Scenario 4: Pumping remains at 2017 conditions, La Reforma is pumped dry in lower reaches

Scenario 4 examined the possibility of overexploitation of Arroyo La Reforma in lower reaches of the stream (where most wells are located, in closest proximity to Todos Santos). The lower 500 m were simulated as dry between the years 2022 and 2027. This resulted in a seawater-freshwater interface migration of 2.6 meters inland in the region of Todos Santos, compared to the previous migration of 0.31 meters (Scenario 1). The lower 750 meters of La Reforma were simulated as dry from 2027 to 2037. This resulted in an interface migration of 16.5 meters inland compared to the previous 0.7 meters (Scenario 1). The interface location in 2037 was simulated at 489 meters from the coastline, compared to 473.2 meters in Scenario 1.

In Punta Lobos, results were not as drastic after removal of RIV cells. The seawater-freshwater interface location in 2037 was simulated at 455 meters from the coastline, whereas in Scenario 1 it was simulated at 454.7 meters.

4.3.3.6 Scenario 5: Pumping remains at 2017 conditions, sea-level rise of 25 mm/yr

The extent of seawater intrusion is worsened when sea-level rise is increased from 4 mm/yr to 25 mm/yr. The simulated seawater-freshwater interface migrates nearly 7 meters inland in comparison to 1.6 meters in Scenario 3. The resulting interface location is at 480 meters from

the coastline in comparison to the previous 474, and reaches up to 510 meters inland at the deepest layer.

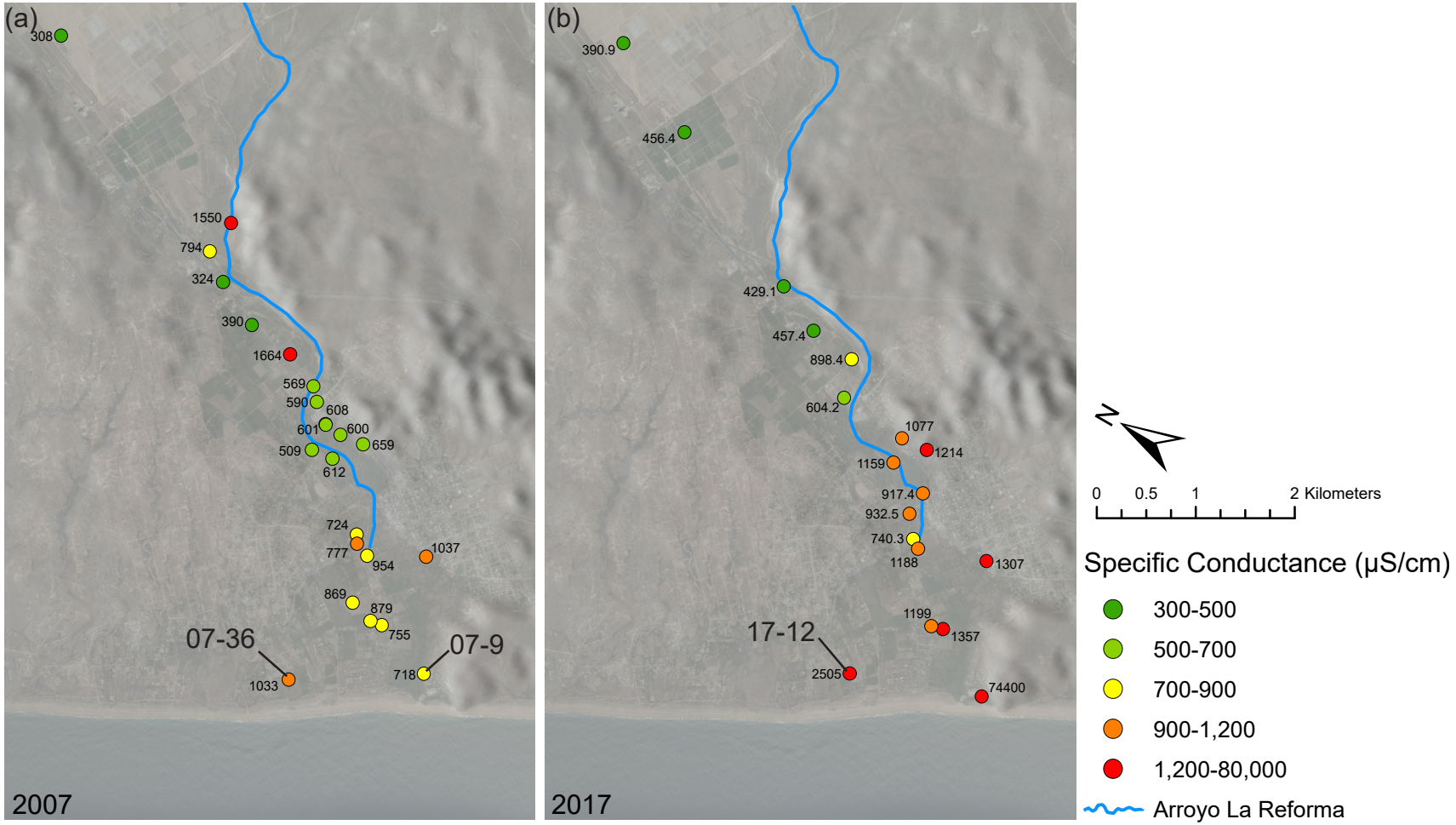

Figure 12: Comparison of specific conductance data collected in (a) 2007 and (b) 2017. Locations of interest include the cluster of wells closest to the coast, showing groundwater values up to 1037 uS/cm in (a) and showing groundwater values up to 2505 uS/cm in (b). Wells labelled 07-36 and 17-12 belong to Susana Mayu, who notified us in June 2017 that salinity in her wells was increasing. Sample location 07-9 was taken from a lower reach of Arroyo La Reforma which previously flowed into La Poza estuary.

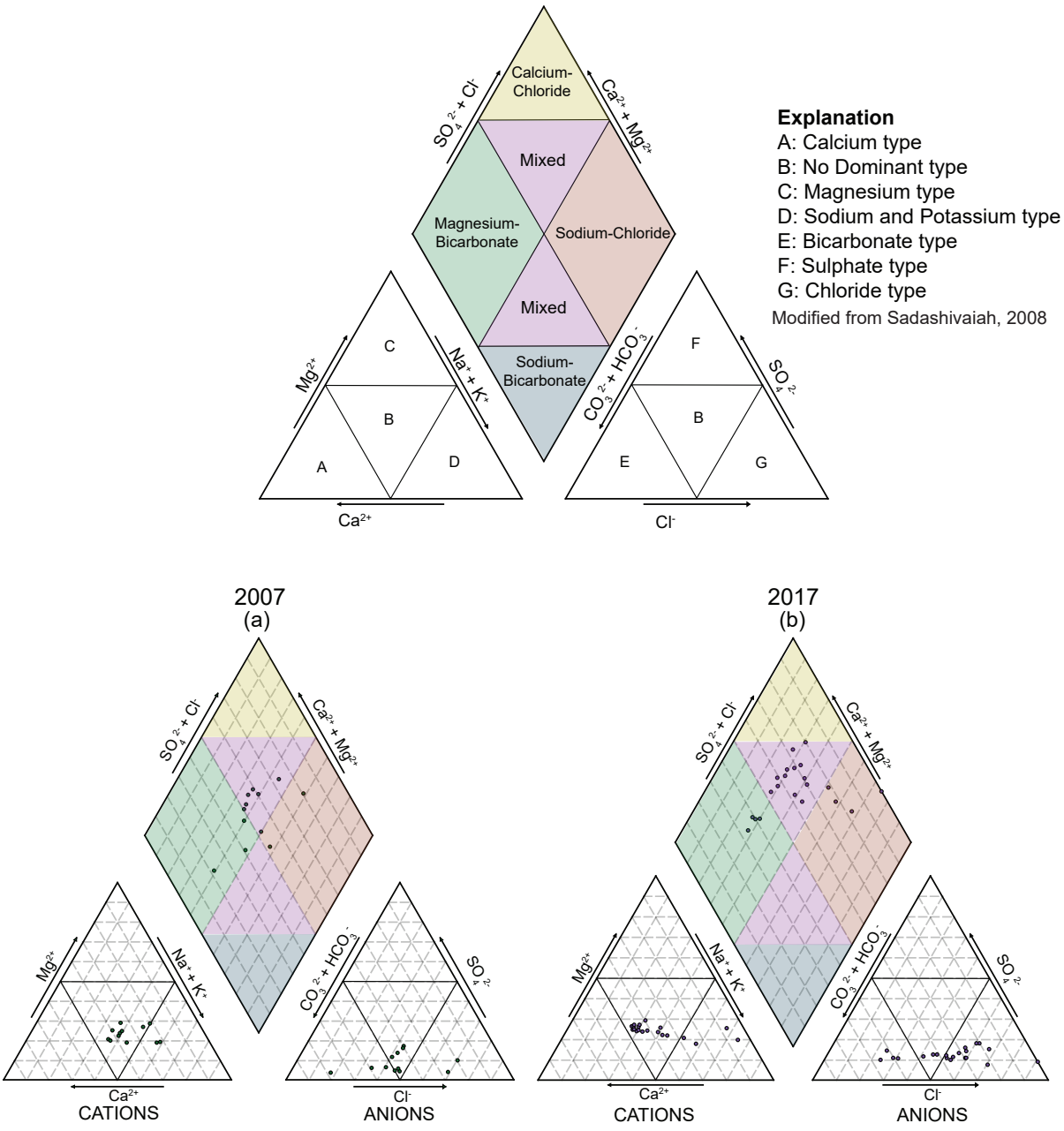

Figure 13: Piper diagrams and associated hydrochemical facies displaying results of major ion analysis for years (a) 2007 and (b) 2017. An increase in sodium-chloride type water can be seen from (a) to (b), as well as an increase in chloride-type water in anion ternary diagrams. Increasing chloride concentration can be seen in the anion ternary diagram displayed in (b). This increase correlates with proximity to the coastline, with the samples plotting with the lowest chloride concentration corresponding to those furthest inland, and samples plotting with the highest chloride concentration corresponding to those located closest to the coastline.

Table 6: Summary of specific conductance data for groundwater samples in 2007 and 2017. Surface water samples, including La Poza Estuary, Las Palmas wetlands, and springs, were not included in statistical calculations.

Specific Conductance Summary		
Year	**2007**	**2017**
Number of samples	22	18
Minimum Value (µS/cm)	308.0	390.9
Maximum Value (µS/cm)	2462.0	4786.0
Mean (µS/cm)	881.3	1209.9
Range (µS/cm)	2154.0	4395.1

Table 7: Hydrochemical facies categories by percentage for 2007 and 2017

Hydrofacies Classification, Todos Santos Aquifer			
Subdivision	**Subdivision Characteristic**	**2007**	**2017**
		Percentage of samples in cateogory	
1	Magnesium-bicarbonate type	25.0	19.0
2	Sodium-chloride type	16.6	19.0
3	Mixed type	58.3	62.0
A	Calcium type	0.0	0.0
B	No Dominant type - (Cation, Anion)	83, 58.3	81, 14.3
C	Magnesium type	0.0	0.0
D	Sodium and potassium type	16.6	19.0
E	Bicarbonate type	25.0	19.0
F	Sulphate type	0.0	0.0
G	Chloride type	16.6	66.7

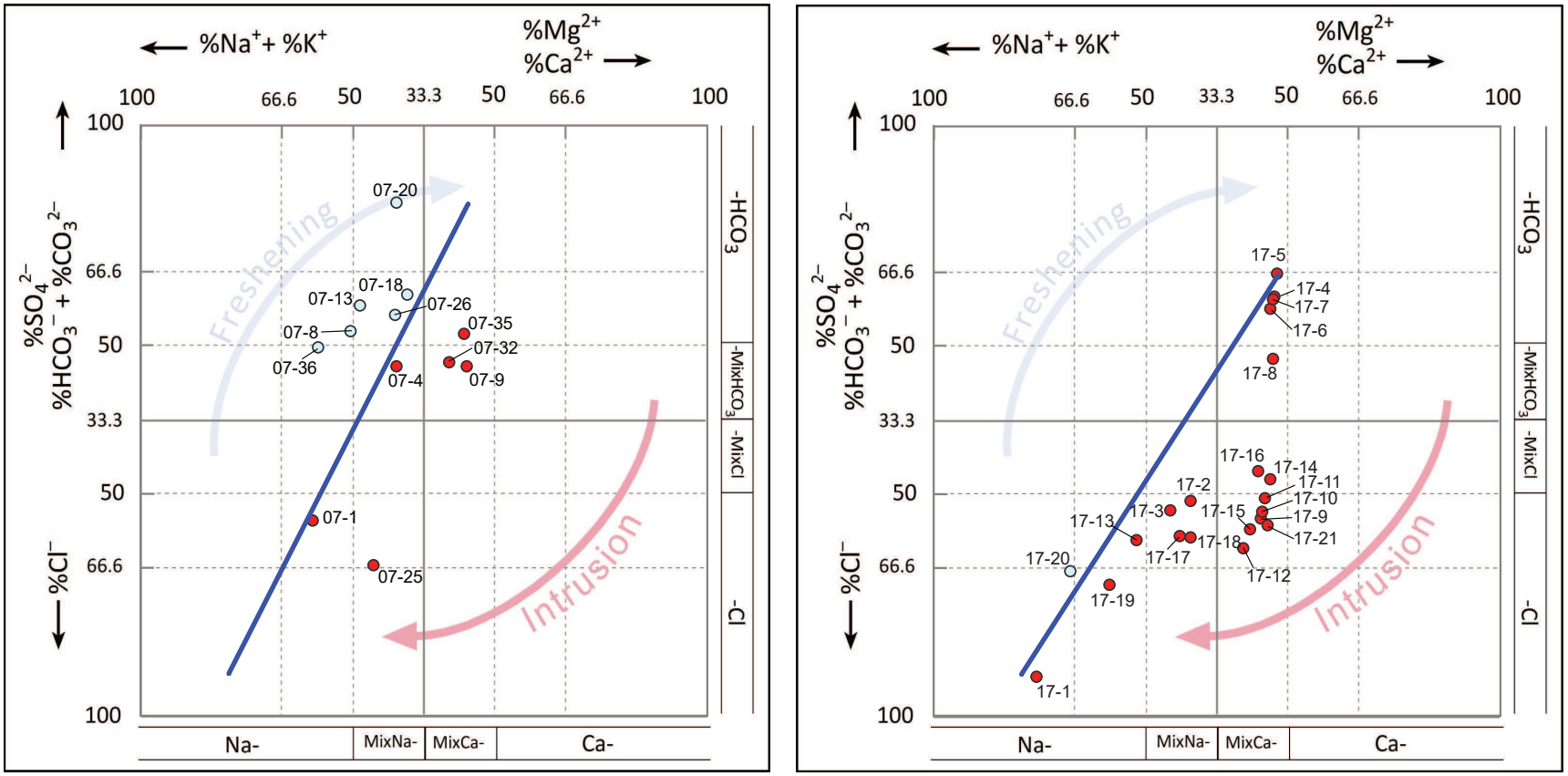

Figure 14: Hydrochemical facies evolution diagrams displayed for years (a) 2007 and (b) 2017 using the excel macro provided by Gimenez-Forcada (2015). Samples in (a) plotted 50% in the freshening phase and 50% in the intrusion phase, while 95% of 2017 samples (b) plotted in the intrusion phase. In (b), many samples plot in the CaCl facies, displaying the characteristic cation exchange of sodium with calcium indicating water which has experienced seawater intrusion. Also in (b), wells geographically located furthest inland (17-4, 17-5, 17-6, 17-7) correspond to samples plotting in the early stages of intrusion and in the freshwater facies, whereas samples from water sources geographically located closest to the coastline (17-1, 17-19, 17-20) correspond to samples plotting in the late stages of intrusion and in the seawater facies.

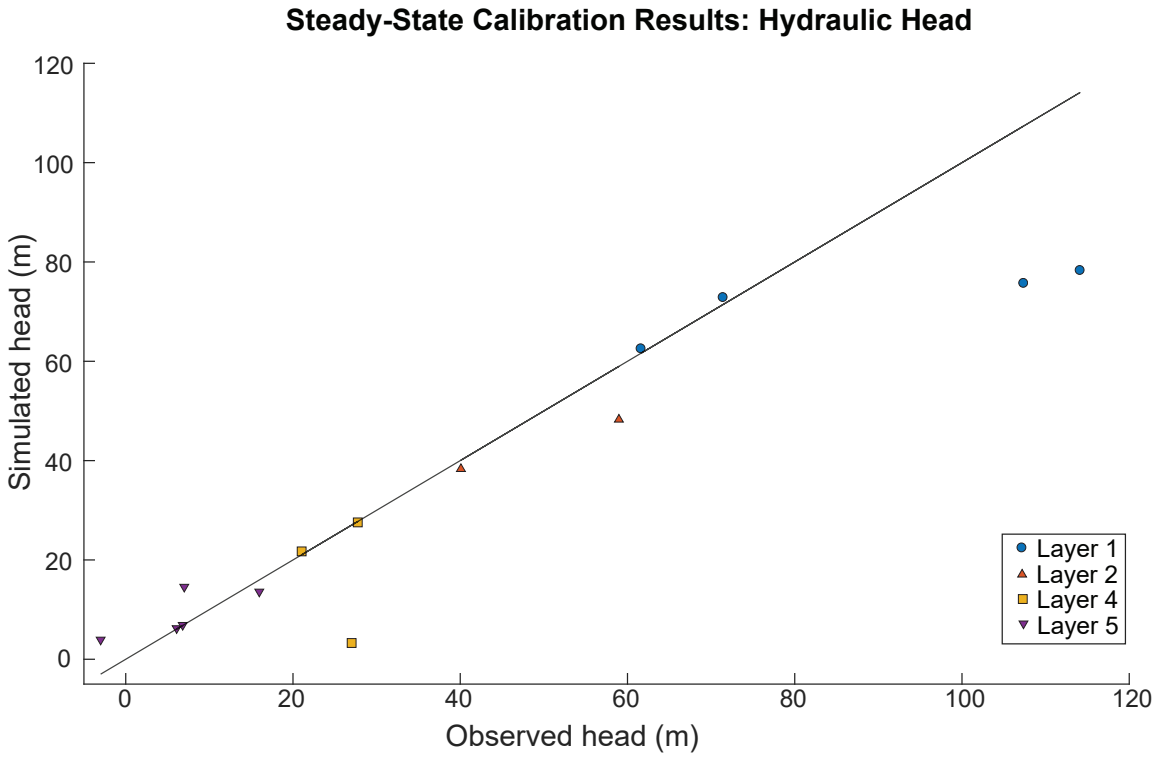

Figure 15: Simulated vs. observed hydraulic head values resulting from steady-state SEAWAT simulation.

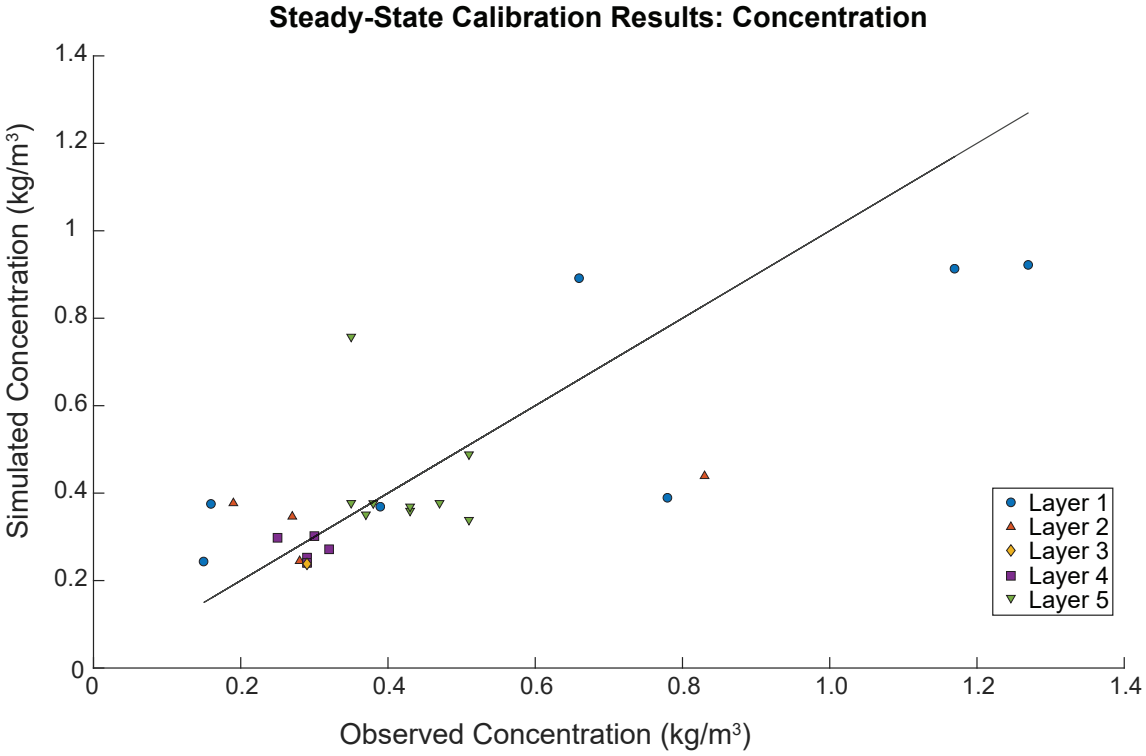

Figure 16: Simulated vs. observed salinity values resulting from steady-state SEAWAT simulation.

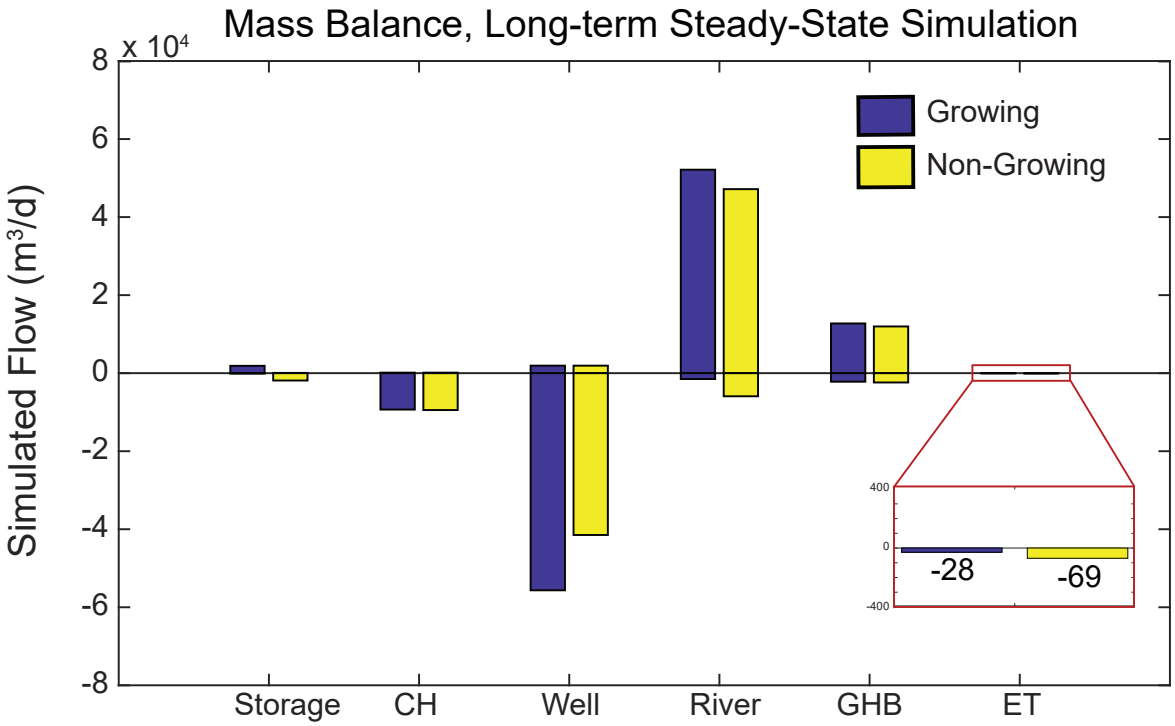

Figure 17: Mass balance summary for long-term steady-state SEAWAT simulation, displaying boundary condition contributions to the aquifer system for growing and non-growing periods. Groundwater inflow from RIV cells takes into account precipitation recharge from large storm events. Groundwater is discharged principally by pumping.

Table 8: Summary of error statistics for steady-state SEAWAT simulation.

Head	No. of Targets	Mean Error (m)	Mean Absolute Error (m)	Root Mean Squared Error (m)	Observed Head Range (m)	Mean Absolute Error / Range (%)	Scaled Root Mean Squared Error (%)
	14	-6.38	8.85	14.86	117.11	7.6	12.7
Concentration	**No. of Targets**	**Mean Error (kg/m^3)**	**Mean Absolute Error (kg/m^3)**	**Root Mean Squared Error (kg/m^3)**	**Observed Concentration Range (kg/m^3)**	**Mean Absolute Error / Range (%)**	**Scaled Root Mean Squared Error (%)**
	26	-0.03	0.13	0.18	1.12	11.5	16.3

Table 9: Mass balance summary for steady-state SEAWAT simulation - mass balance results are presented for final time steps corresponding to final growing and non-growing stress periods.

	Stress Period 150, Time Step 1 Growing		Stress Period 149, Time Step 1 Non-Growing	
	Inflow (m^3/d)	**Outflow (m^3/d)**	**Inflow (m^3/d)**	**Outflow (m^3/d)**
Storage	1,878.16	-83.61	62.78	-1,882.69
Constant Head	133.28	-9,327.43	131.47	-9,451.91
Wells	1,922.76	-55,652.12	1,922.76	-41,473.80
River	52,147.91	-1,501.32	47,165.43	-5,925.22
General Head	12,739.32	-2,190.29	11,970.42	-2,387.74
Evapotranspiration	0.00	-28.43	0.00	-69.48

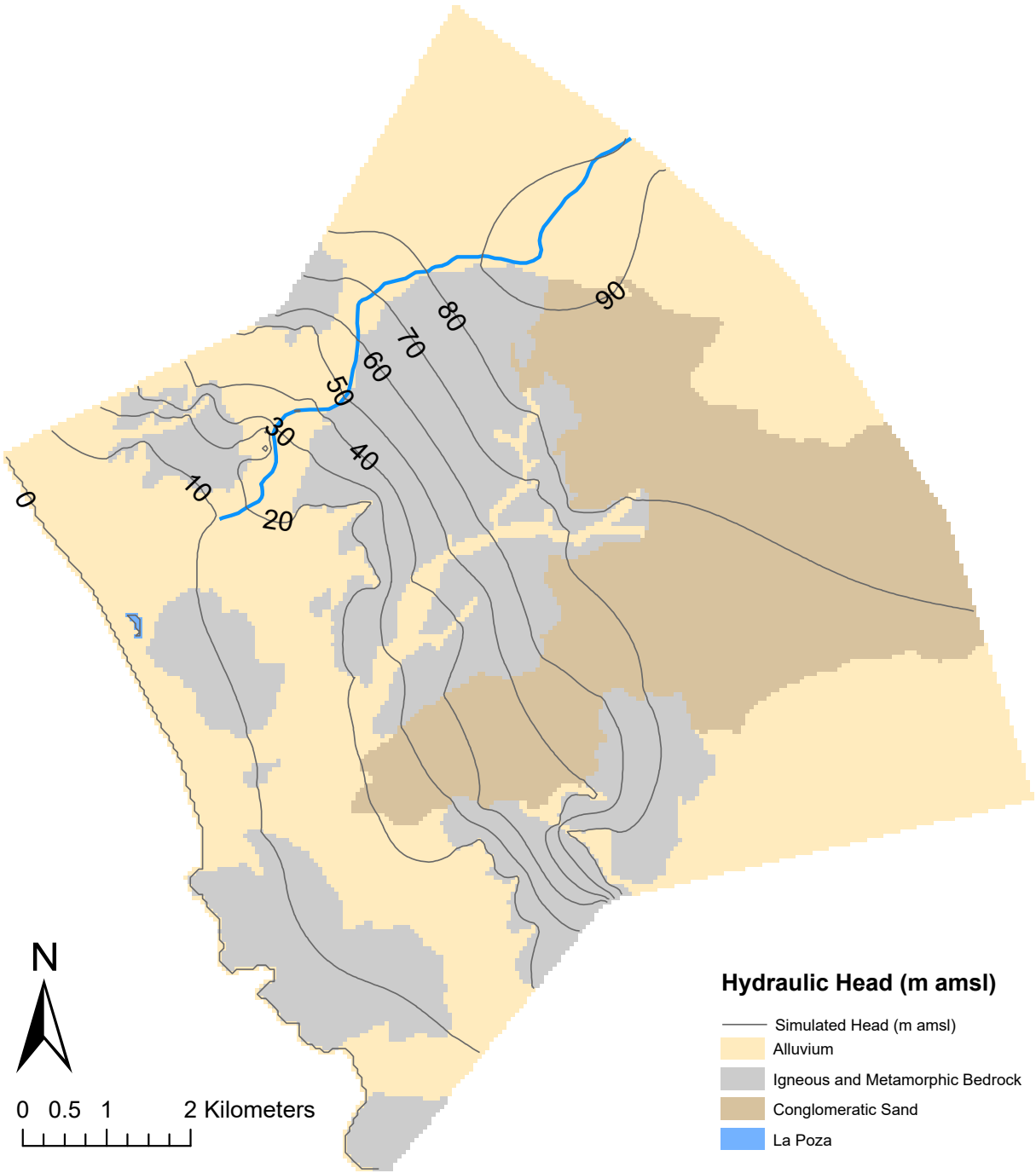

Figure 18: Simulated hydraulic head potentiometric surface map displaying 2007 hydrogeologic conditions. Groundwater flow is from northeast to southwest, consistent with topographic driven flow from the Sierra de la Laguna mountains to the Pacific Ocean.

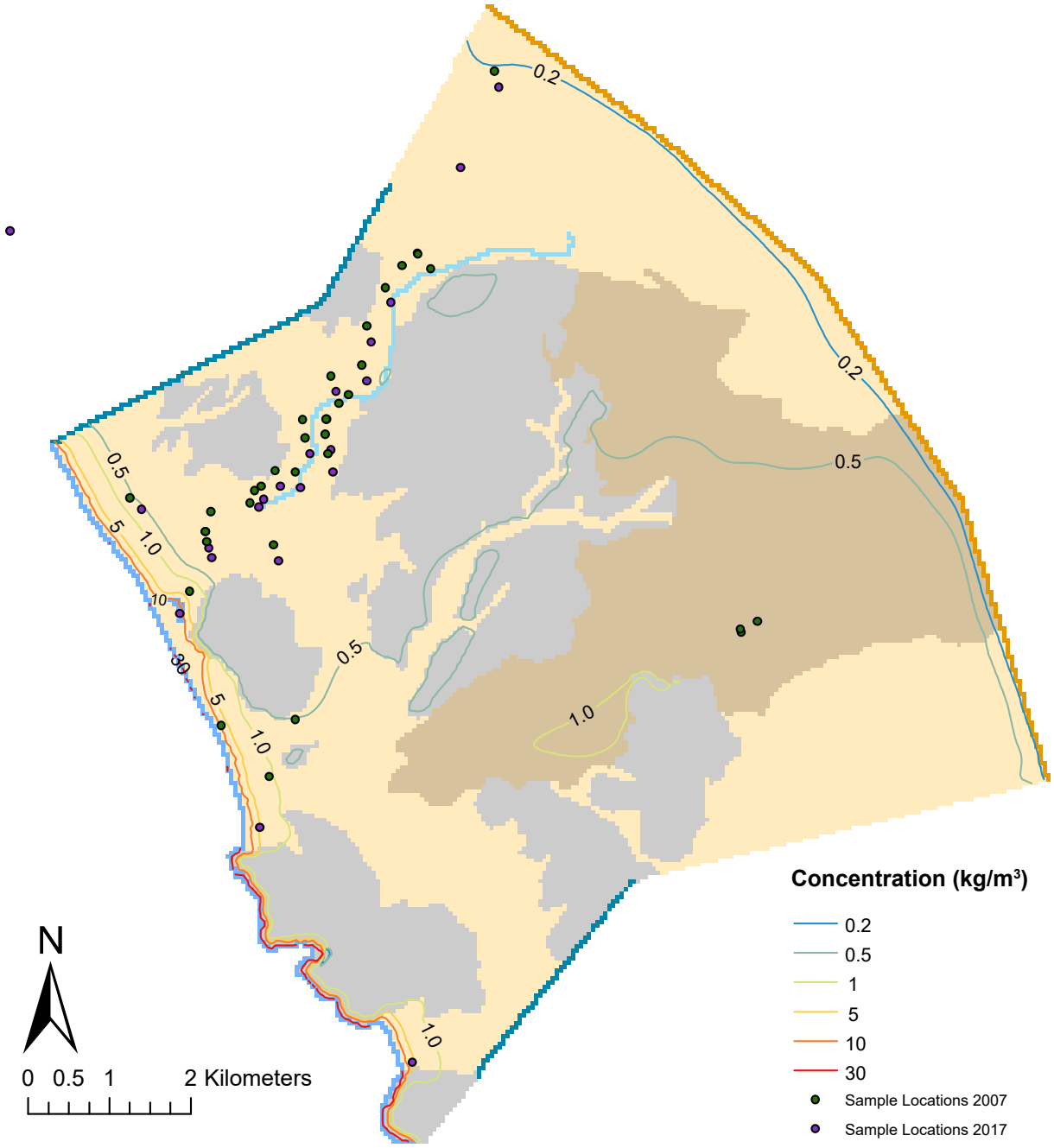

Figure 19: Simulated salinity contour map displaying results from layer 5 of the steady-state SEAWAT simulation. The seawater-freshwater interface, located at contour 1.0 kg/m^3, reaches up to 607 meters inland. A high salinity gradient can be seen near the coastline. Six sample locations can be seen having already experienced salinities higher than 1.0 kg/m^3 by 2007.

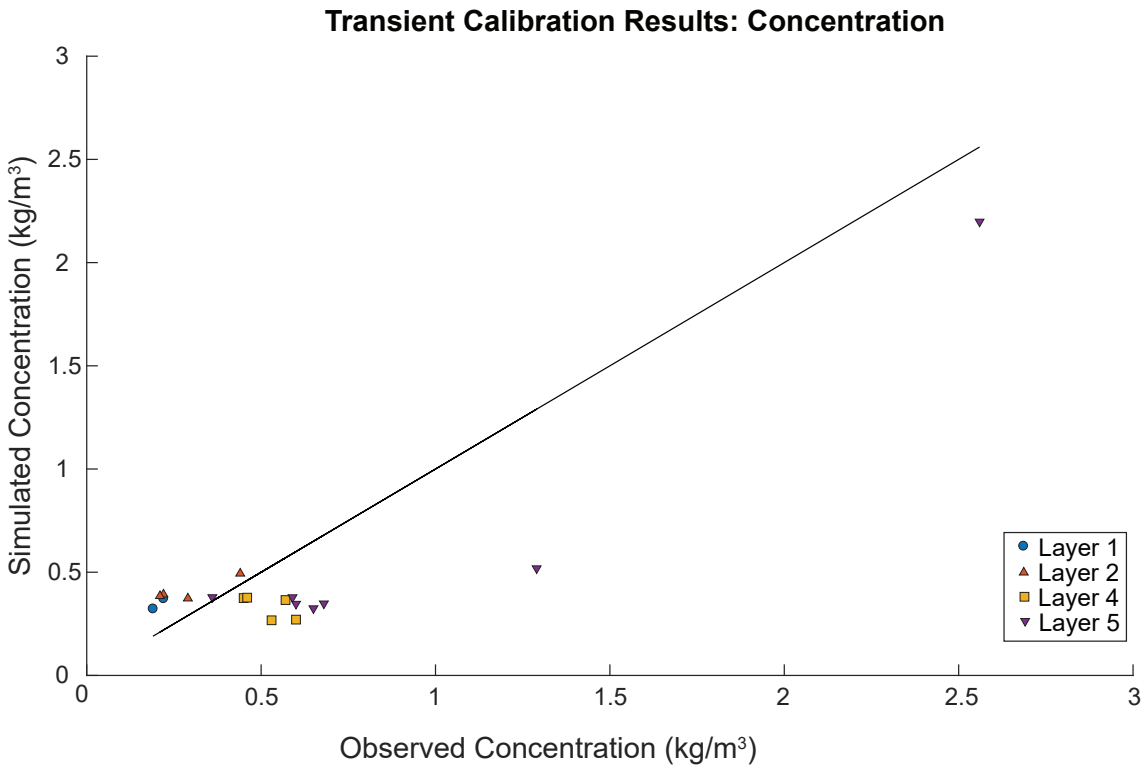

Figure 20: Simulated vs. observed salinity values for transient SEAWAT simulation for years 2007-2017.

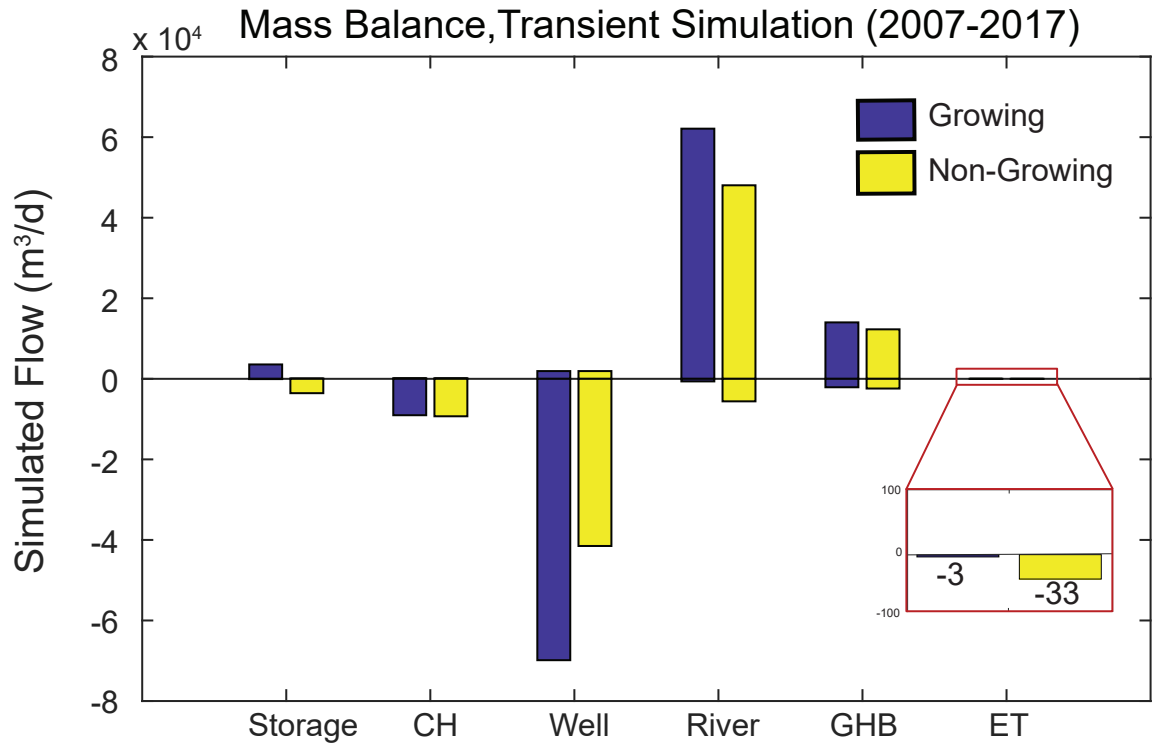

Figure 21: Mass balance summary for transient 2007-2017 SEAWAT simulation, displaying boundary condition contributions to the aquifer system for growing and non-growing periods.

Table 10: Summary of error statistics for transient 2007-2017 SEAWAT simulation.

Concentration	No. of Targets	Mean Error (kg/m^3)	Mean Absolute Error (kg/m^3)	Root Mean Squared Error (kg/m^3)	Observed Concentration Range (kg/m^3)	Mean Absolute Error / Range (%)	Scaled Root Mean Squared Error (%)
	18	-0.13	0.22	0.28	2.37	9.4	11.8

Table 11: Mass balance summary for transient 2007-2017 SEAWAT simulation - mass balance results are presented for final time steps corresponding to final growing and non-growing stress periods.

Transient Model Mass Balance

	Stress Period 20, Time Step 6 Growing		Stress Period 19, Time Step 6 Non-Growing	
	Inflow (m^3/d)	**Outflow (m^3/d)**	**Inflow (m^3/d)**	**Outflow (m^3/d)**
Storage	3,569.44	-67.56	70.13	-3,563.05
Constant Head	132.59	-9,036.54	128.14	-9,300.35
Wells	1,922.76	-69,859.24	1,922.76	-41,502.60
River	62,108.80	-638.57	48,048.82	-5,592.65
General Head	14,010.22	-2,095.24	12,286.89	-2,411.50
Evapotranspiration	0.00	-2.67	0.00	-32.77

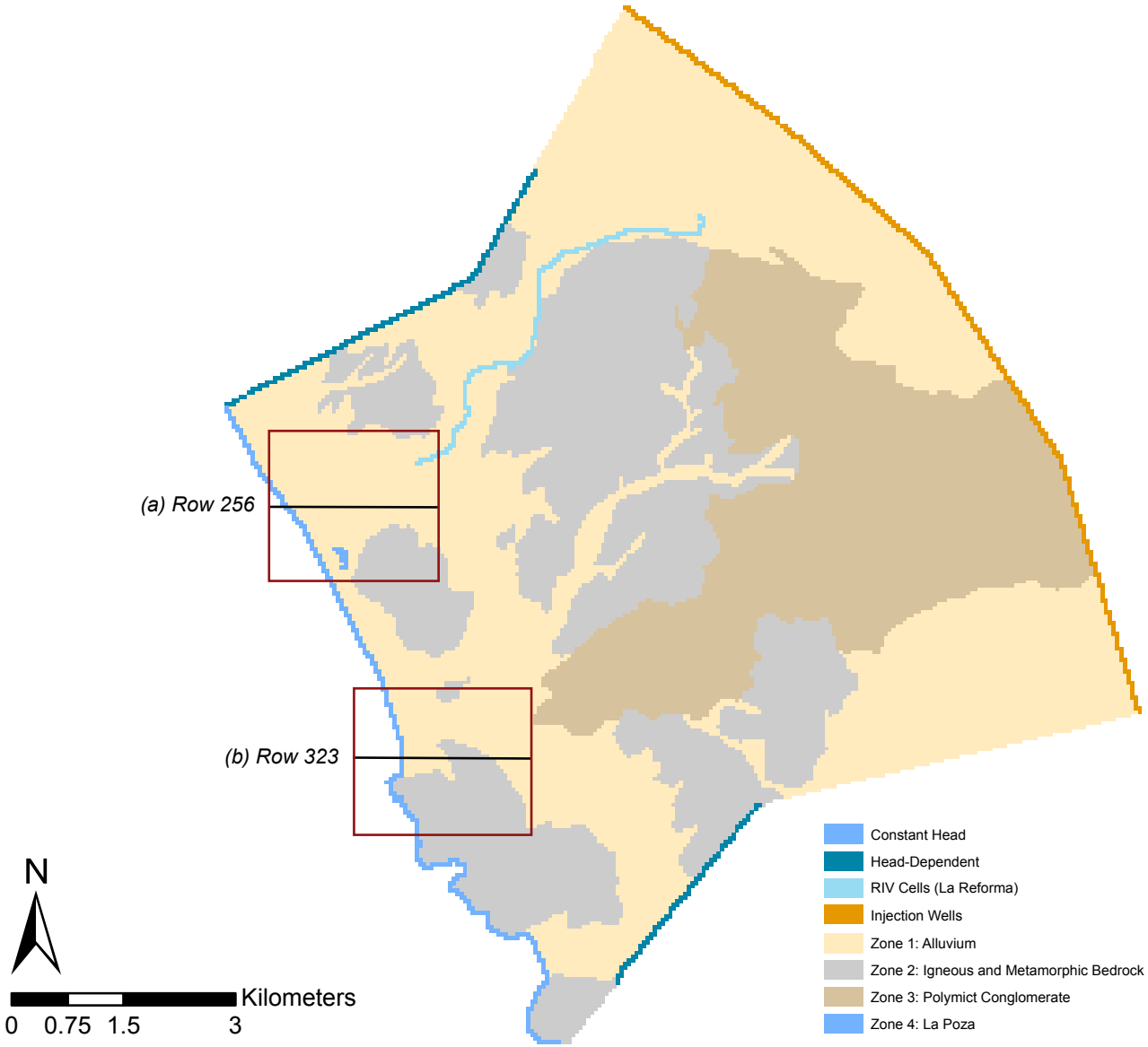

Figure 22: Locations of cross-section profiles for area (a) Todos Santos and (b) Punta Lobos, where simulated seawater-freshwater interface was plotted with depth (Fig. 23). Red boxes show extent of plan view salinity contour maps displayed in Figure 23.

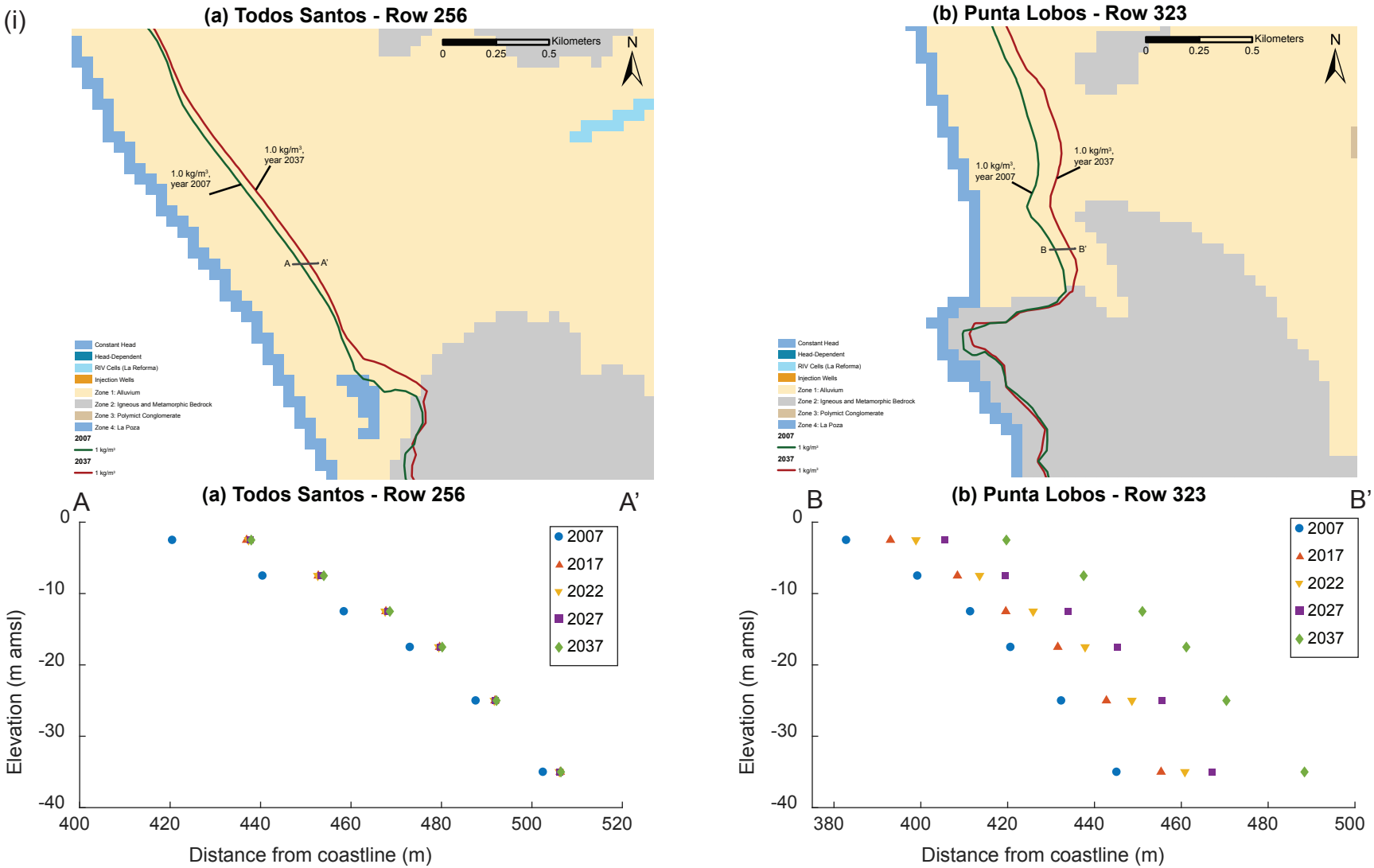

Figure 23: Simulated seawater-freshwater interface location (identified at salinity value of 1.0 kg/m3) in plan view for years 2007 and 2037, model layer 5, and with depth at the end of years 2007, 2017, 2022, 2027, and 2037 for locations (a) Todos Santos town and (b) Punta Lobos beach (Fig. 22). Results for the following five forecasting scenarios are displayed: (i) Pumping rates remain at 2007 conditions, (ii) Pumping rates are doubled in all wells, (iii) Pumping rates remain at 2017 conditions, sea-level rise of 4 mm/yr, (iv) Pumping rates remain at 2017 conditions, Arroyo La Reforma is overexploited in lower reaches, and (v) Pumping rates remain at 2017 conditions, sea-level rise of 25 mm/yr.

(ii)

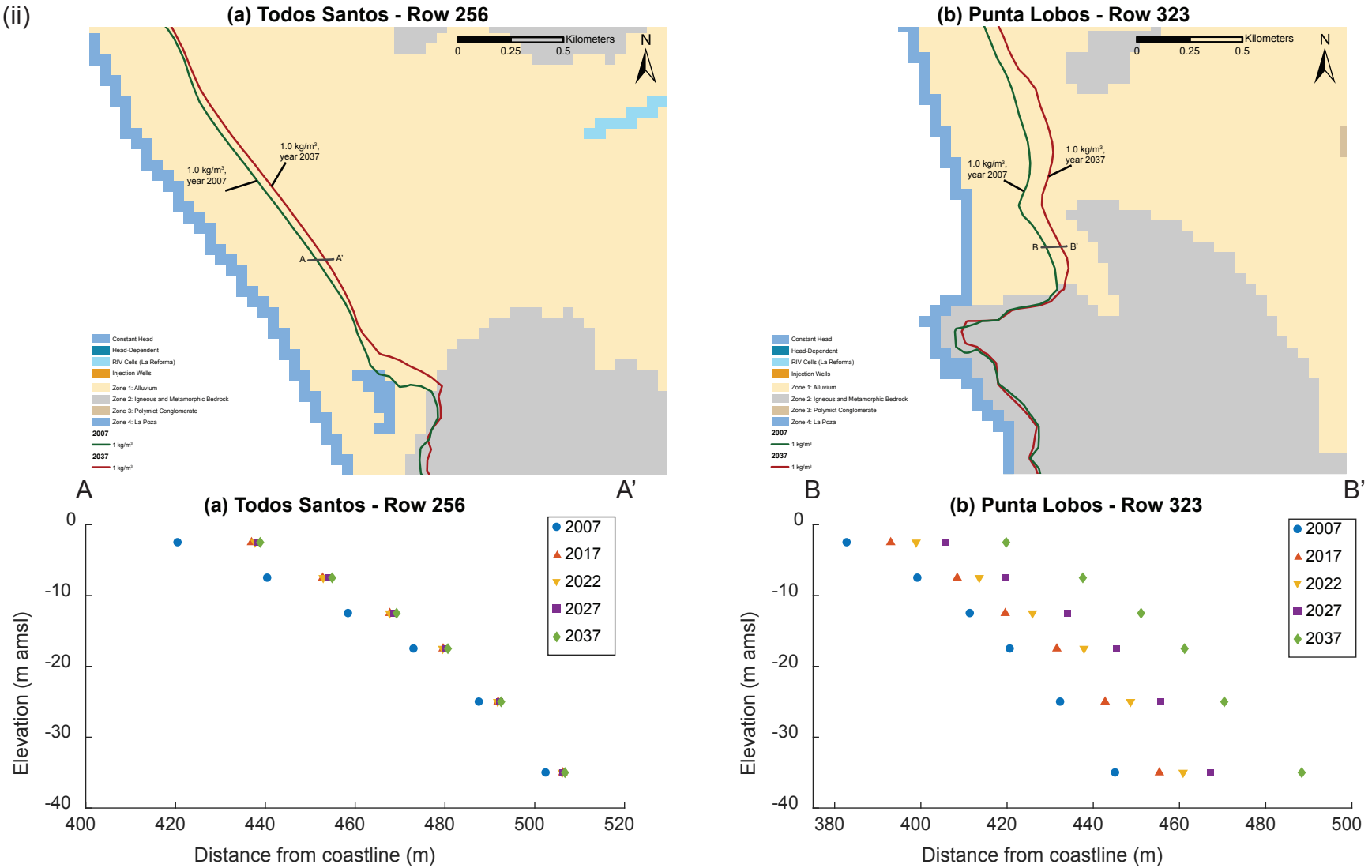

Figure 23: Simulated seawater-freshwater interface location (identified at salinity value of 1.0 kg/m3) in plan view for years 2007 and 2037, model layer 5, and with depth at the end of years 2007, 2017, 2022, 2027, and 2037 for locations (a) Todos Santos town and (b) Punta Lobos beach (Fig. 22). Results for the following five forecasting scenarios are displayed: (i) Pumping rates remain at 2007 conditions, (ii) Pumping rates are doubled in all wells, (iii) Pumping rates remain at 2017 conditions, sea-level rise of 4 mm/yr, (iv) Pumping rates remain at 2017 conditions, Arroyo La Reforma is overexploited in lower reaches, and (v) Pumping rates remain at 2017 conditions, sea-level rise of 25 mm/yr.

(iii)

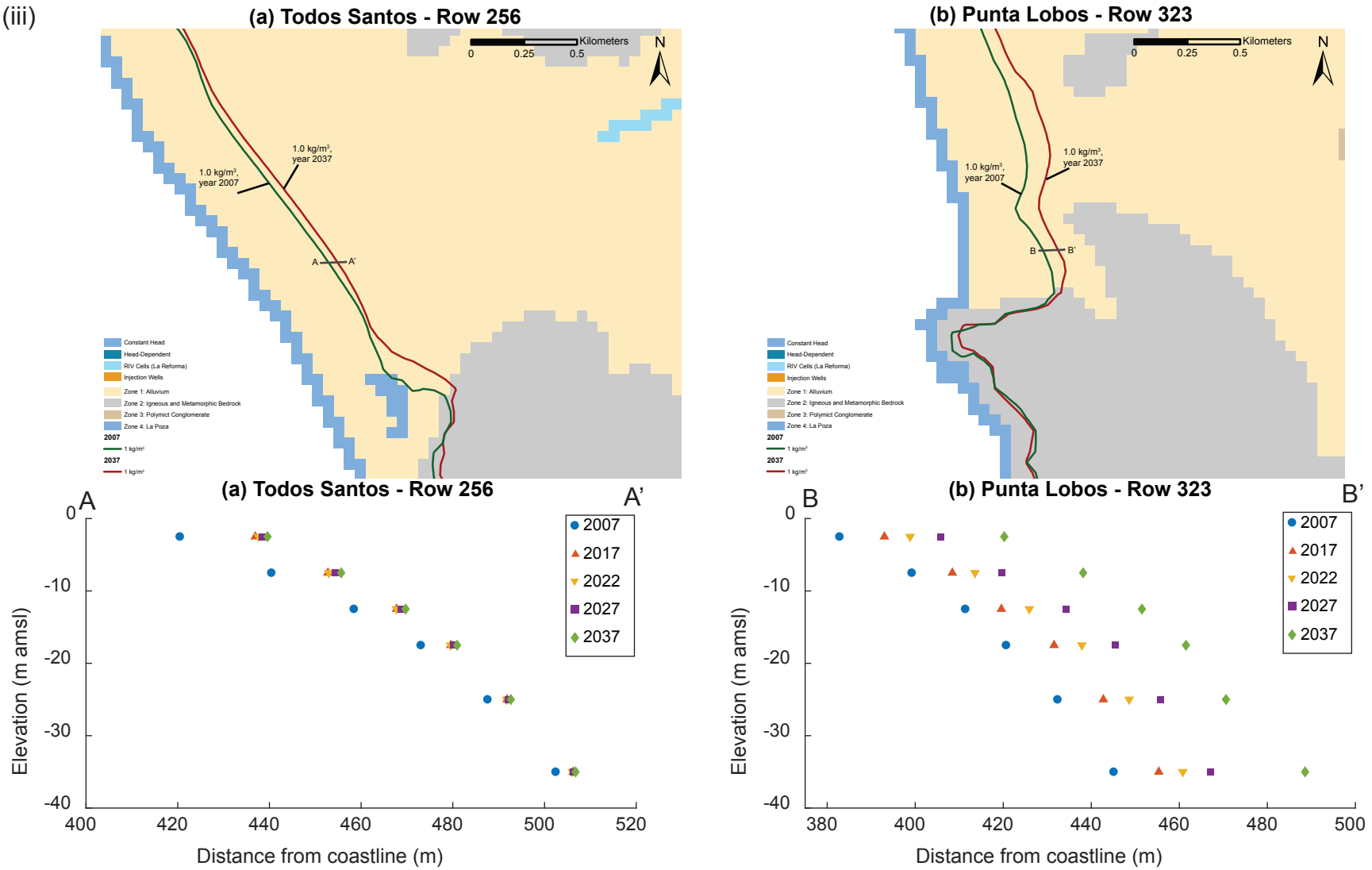

Figure 23: Simulated seawater-freshwater interface location (identified at salinity value of 1.0 kg/m3) in plan view for years 2007 and 2037, model layer 5, and with depth at the end of years 2007, 2017, 2022, 2027, and 2037 for locations (a) Todos Santos town and (b) Punta Lobos beach (Fig. 22). Results for the following five forecasting scenarios are displayed: (i) Pumping rates remain at 2007 conditions, (ii) Pumping rates are doubled in all wells, (iii) Pumping rates remain at 2017 conditions, sea-level rise of 4 mm/yr, (iv) Pumping rates remain at 2017 conditions, Arroyo La Reforma is overexploited in lower reaches, and (v) Pumping rates remain at 2017 conditions, sea-level rise of 25 mm/yr.

(iv)

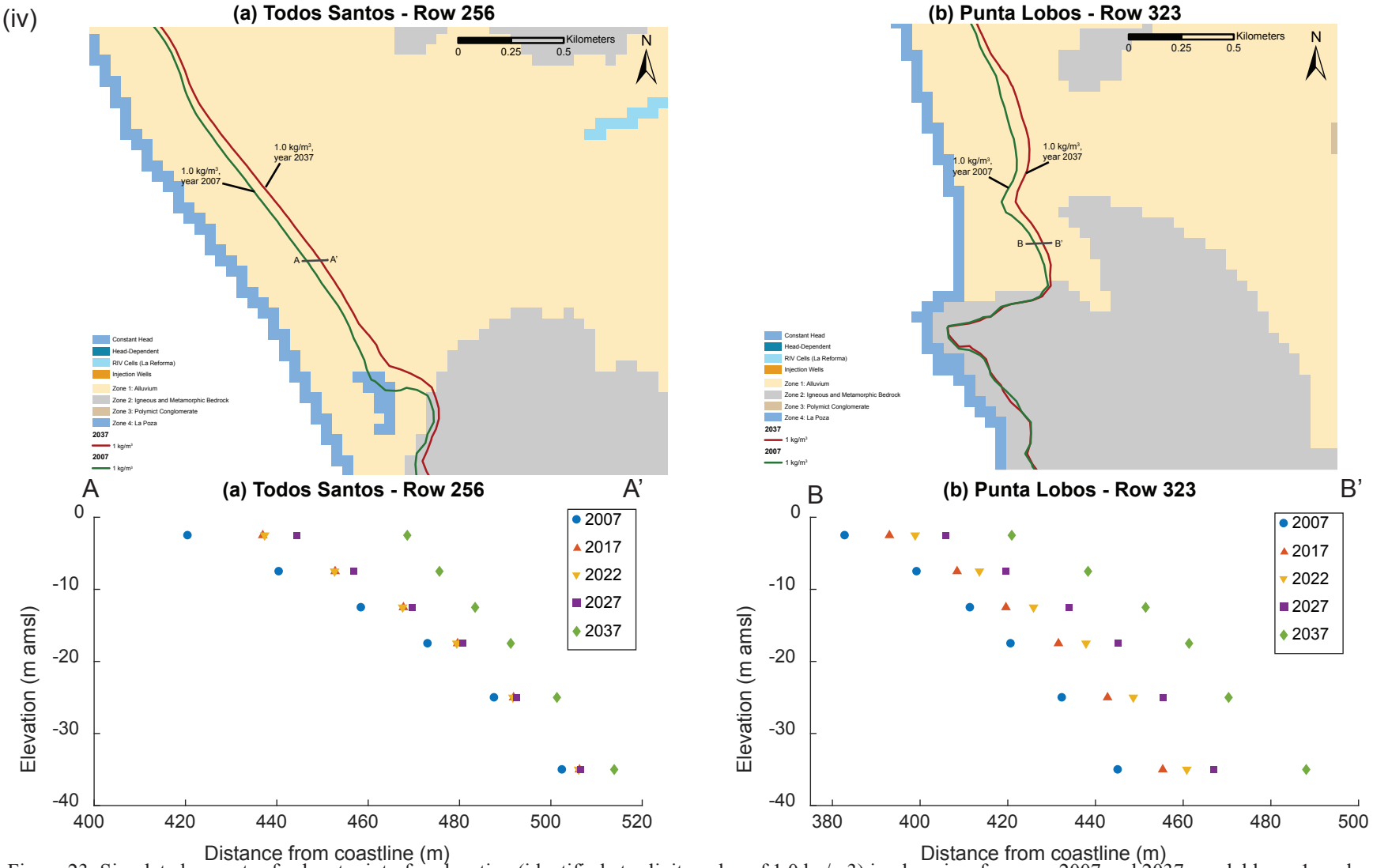

Figure 23: Simulated seawater-freshwater interface location (identified at salinity value of 1.0 kg/m3) in plan view for years 2007 and 2037, model layer 1, and with depth at the end of years 2007, 2017, 2022, 2027, and 2037 for locations (a) Todos Santos town and (b) Punta Lobos beach (Fig. 22). Results for the following five forecasting scenarios are displayed: (i) Pumping rates remain at 2007 conditions, (ii) Pumping rates are doubled in all wells, (iii) Pumping rates remain at 2017 conditions, sea-level rise of 4 mm/yr, (iv) Pumping rates remain at 2017 conditions, Arroyo La Reforma is overexploited in lower reaches, and (v) Pumping rates remain at 2017 conditions, sea-level rise of 25 mm/yr.

(v)

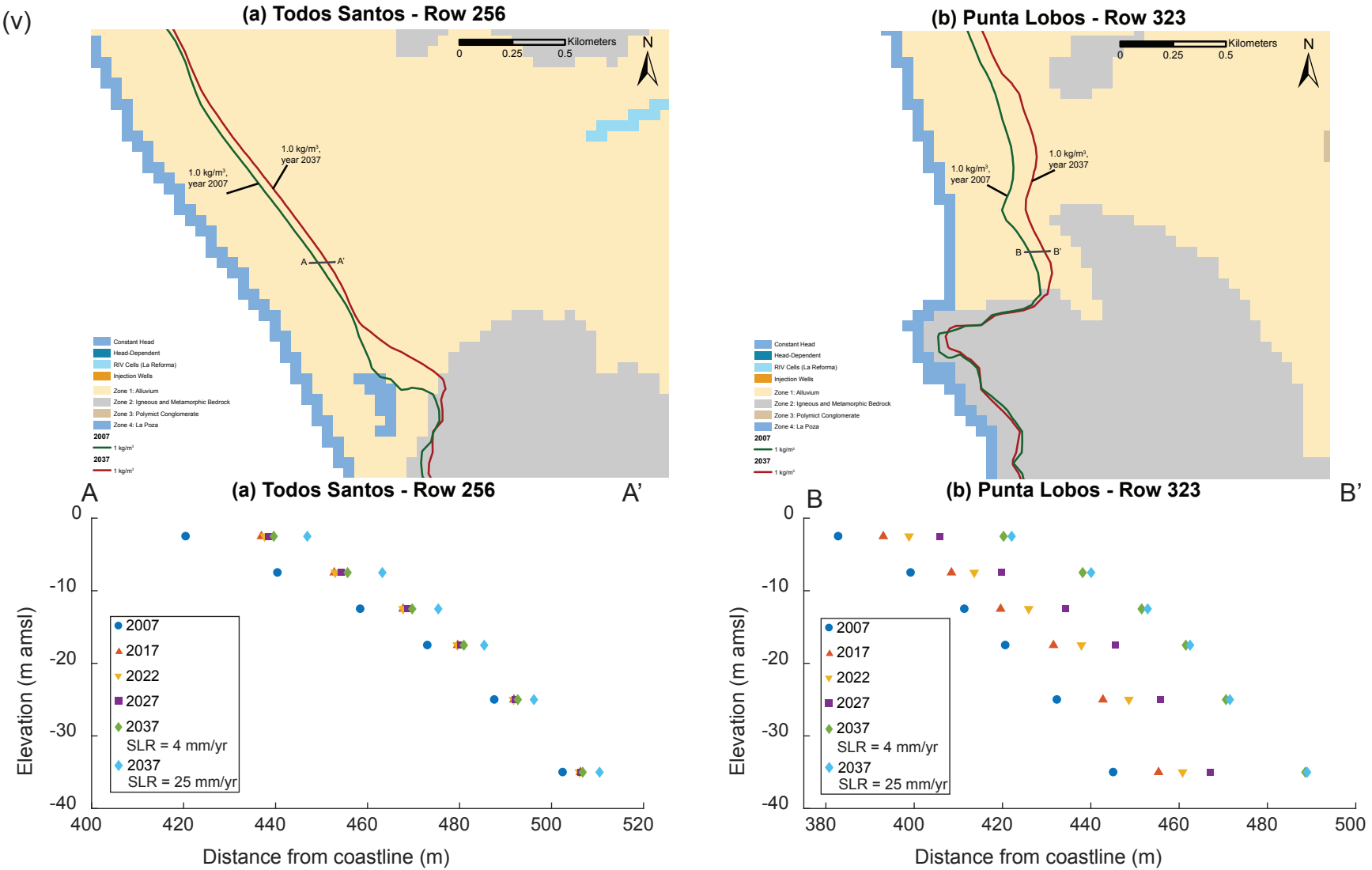

Figure 23: Simulated seawater-freshwater interface location (identified at salinity value of 1.0 kg/m3) in plan view for years 2007 and 2037, model layer 5, and with depth at the end of years 2007, 2017, 2022, 2027, and 2037 for locations (a) Todos Santos town and (b) Punta Lobos beach (Fig. 22). Results for the following five forecasting scenarios are displayed: (i) Pumping rates remain at 2007 conditions, (ii) Pumping rates are doubled in all wells, (iii) Pumping rates remain at 2017 conditions, sea-level rise of 4 mm/yr, (iv) Pumping rates remain at 2017 conditions, Arroyo La Reforma is overexploited in lower reaches, and (v) Pumping rates remain at 2017 conditions, sea-level rise of 25 mm/yr.

Table 12: Simulated seawater-freshwater interface model results for steady-state, transient ('07-'17), and forecasting scenarios for 5, 10, and 20 years. Results are listed for the following locations: (a) Todos Santos town area, and (b) Punta Lobos beach, and for the following forecasting scenarios: (i) Pumping rates remain at 2007 conditions, (ii) Pumping rates are doubled in all wells, (iii) Pumping rates remain at 2017 conditions, sea-level rise of 4 mm/yr, (iv) Pumping rates remain at 2017 conditions, Arroyo La Reforma is overexploited in lower reaches, and (v) Pumping rates remain at 2017 conditions, sea-level rise of 25 mm/yr.

(i)

(a) Todos Santos - Row 256

Year	2007	2017	2022	2027	2037				
Simulated Depth (m amsl)	Simulated distance from coastline (m)					Simulated Depth (m amsl)	Evolution from 2017 to 2022 (m)	Evolution from 2017 to 2027 (m)	Evolution from 2017 to 2037 (m)
-2.5	420.47	436.92	437.33	437.64	437.94	-2.5	0.41	0.72	1.02
-7.5	440.43	452.76	452.65	453.43	453.98	-7.5	-0.11	0.67	1.22
-12.5	458.43	467.72	467.55	468.09	468.59	-12.5	-0.17	0.38	0.87
-17.5	473.02	479.58	479.41	479.77	480.17	-17.5	-0.18	0.19	0.59
-25	487.58	491.84	491.69	491.88	492.17	-25	-0.15	0.05	0.33
-35	502.44	506.26	506.08	506.15	506.42	-35	-0.19	-0.12	0.15
Average Distance from Coastline (m)	463.73	472.51	472.45	472.83	473.21	Average Migration Inland (m)	-0.06	0.31	0.70

(b) Punta Lobos - Row 323

Year	2007	2017	2022	2027	2037				
Simulated Depth (m amsl)	Simulated distance from coastline (m)					Simulated Depth (m amsl)	Evolution from 2017 to 2022 (m)	Evolution from 2017 to 2027 (m)	Evolution from 2017 to 2037 (m)
-2.5	382.81	393.00	398.88	405.51	419.71	-2.5	5.87	12.50	26.71
-7.5	399.22	408.43	413.53	419.47	437.51	-7.5	5.10	11.04	29.07
-12.5	411.39	419.58	425.87	433.94	451.04	-12.5	6.30	14.36	31.46
-17.5	420.66	431.55	437.84	445.27	461.16	-17.5	6.29	13.72	29.61
-25	432.34	442.75	448.62	455.53	470.39	-25	5.87	12.78	27.64
-35	445.09	455.34	460.83	467.05	488.37	-35	5.48	11.71	33.03
Average Distance from Coastline (m)	415.25	425.11	430.93	437.79	454.70	Average Migration Inland (m)	5.82	12.68	29.59

(ii)

(a) Todos Santos - Row 256

Year	2007	2017	2022	2027	2037				
Simulated Depth (m amsl)	Simulated distance from coastline (m)					Simulated Depth (m amsl)	Evolution from 2017 to 2022 (m)	Evolution from 2017 to 2027 (m)	Evolution from 2017 to 2037 (m)
-2.5	420.47	436.92	437.70	438.32	438.84	-2.5	0.78	1.40	1.92
-7.5	440.43	452.76	452.88	454.05	454.88	-7.5	0.12	1.29	2.12
-12.5	458.43	467.72	467.68	468.51	469.22	-12.5	-0.04	0.79	1.50
-17.5	473.02	479.58	479.50	480.08	480.65	-17.5	-0.09	0.50	1.07
-25	487.58	491.84	491.74	492.09	492.51	-25	-0.09	0.26	0.68
-35	502.44	506.26	506.11	506.32	506.73	-35	-0.15	0.06	0.46
Average Distance from Coastline (m)	463.73	472.51	472.60	473.23	473.81	Average Migration Inland (m)	0.09	0.71	1.29

(b) Punta Lobos - Row 323

Year	2007	2017	2022	2027	2037				
Simulated Depth (m amsl)	Simulated distance from coastline (m)					Simulated Depth (m amsl)	Evolution from 2017 to 2022 (m)	Evolution from 2017 to 2027 (m)	Evolution from 2017 to 2037 (m)
-2.5	382.81	393.00	398.90	405.61	419.80	-2.5	5.90	12.61	26.79
-7.5	399.22	408.43	413.55	419.55	437.59	-7.5	5.11	11.12	29.15
-12.5	411.39	419.58	425.90	434.04	451.09	-12.5	6.32	14.47	31.51
-17.5	420.66	431.55	437.86	445.37	461.19	-17.5	6.31	13.82	29.64
-25	432.34	442.75	448.64	455.62	470.41	-25	5.89	12.87	27.66
-35	445.09	455.34	460.84	467.13	488.37	-35	5.50	11.79	33.03
Average Distance from Coastline (m)	415.25	425.11	430.95	437.89	454.74	Average Migration Inland (m)	5.84	12.78	29.63

Table 12 cont.:

(iii)

(a) Todos Santos - Row 256

Year	2007	2017	2022	2027	2037	Simulated Depth (m amsl)	Evolution from 2017 to 2022 (m)	Evolution from 2017 to 2027 (m)	Evolution from 2017 to 2037 (m)
Simulated Depth (m amsl)	Simulated distance from coastline (m)								
-2.5	420.47	437.15	437.60	438.51	439.60	-2.5	0.45	1.36	2.44
-7.5	440.43	453.02	452.95	454.33	455.65	-7.5	-0.06	1.31	2.63
-12.5	458.43	467.88	467.73	468.69	469.70	-12.5	-0.15	0.81	1.82
-17.5	473.02	479.68	479.51	480.18	480.93	-17.5	-0.17	0.50	1.25
-25	487.58	491.89	491.74	492.13	492.66	-25	-0.15	0.24	0.77
-35	502.44	506.27	506.07	506.30	506.76	-35	-0.20	0.03	0.49
Average Distance from Coastline (m)	463.73	472.65	472.60	473.36	474.22	**Average Migration Inland (m)**	-0.05	0.71	1.57

(b) Punta Lobos - Row 323

Year	2007	2017	2022	2027	2037	Simulated Depth (m amsl)	Evolution from 2017 to 2022 (m)	Evolution from 2017 to 2027 (m)	Evolution from 2017 to 2037 (m)
Simulated Depth (m amsl)	Simulated distance from coastline (m)								
-2.5	382.81	393.03	398.83	405.80	420.23	-2.5	5.80	12.77	27.20
-7.5	399.22	408.51	413.59	419.77	438.16	-7.5	5.08	11.25	29.64
-12.5	411.39	419.63	425.93	434.27	451.51	-12.5	6.30	14.64	31.88
-17.5	420.66	431.61	437.87	445.52	461.51	-17.5	6.26	13.92	29.91
-25	432.34	442.77	448.61	455.68	470.61	-25	5.84	12.91	27.84
-35	445.09	455.34	460.80	467.12	488.58	-35	5.45	11.78	33.24
Average Distance from Coastline (m)	415.25	425.15	430.94	438.03	455.10	**Average Migration Inland (m)**	5.79	12.88	29.95

(iv)

(a) Todos Santos - Row 256

Year	2007	2017	2022	2027	2037	Simulated Depth (m amsl)	Evolution from 2017 to 2022 (m)	Evolution from 2017 to 2027 (m)	Evolution from 2017 to 2037 (m)
Simulated Depth (m amsl)	Simulated distance from coastline (m)								
-2.5	420.47	436.92	437.33	444.43	468.56	-2.5	0.41	7.51	31.64
-7.5	440.43	452.76	452.65	456.76	475.60	-7.5	-0.11	4.00	22.84
-12.5	458.43	467.72	467.55	469.72	483.42	-12.5	-0.17	2.00	15.70
-17.5	473.02	479.58	479.41	480.79	491.22	-17.5	-0.18	1.21	11.63
-25	487.58	491.84	491.69	492.44	501.33	-25	-0.15	0.60	9.50
-35	502.44	506.26	506.08	506.54	513.87	-35	-0.19	0.27	7.61
Average Distance from Coastline (m)	463.73	472.51	472.45	475.11	489.00	**Average Migration Inland (m)**	-0.06	2.60	16.49

(b) Punta Lobos - Row 323

Year	2007	2017	2022	2027	2037	Simulated Depth (m amsl)	Evolution from 2017 to 2022 (m)	Evolution from 2017 to 2027 (m)	Evolution from 2017 to 2037 (m)
Simulated Depth (m amsl)	Simulated distance from coastline (m)								
-2.5	382.81	393.00	398.88	405.77	420.91	-2.5	5.87	12.76	27.90
-7.5	399.22	408.43	413.53	419.48	438.30	-7.5	5.10	11.04	29.87
-12.5	411.39	419.58	425.87	433.91	451.44	-12.5	6.30	14.33	31.87
-17.5	420.66	431.55	437.84	445.24	461.34	-17.5	6.29	13.69	29.79
-25	432.34	442.75	448.62	455.49	470.36	-25	5.87	12.74	27.61
-35	445.09	455.34	460.83	467.02	488.07	-35	5.48	11.67	32.73
Average Distance from Coastline (m)	415.25	425.11	430.93	437.82	455.07	**Average Migration Inland (m)**	5.82	12.71	29.96

Table 12 cont.

(v)

(a) Todos Santos - Row 256

Year	2007	2017	2037		
Simulated Depth (m amsl)	Simulated distance from coastline (m)			Simulated Depth (m amsl)	Evolution from 2017 to 2037 (m)
-2.5	420.47	436.92	446.90	-2.5	9.98
-7.5	440.43	452.76	463.20	-7.5	10.44
-12.5	458.43	467.72	475.37	-12.5	7.65
-17.5	473.02	479.58	485.35	-17.5	5.77
-25	487.58	491.84	496.16	-25	4.33
-35	502.44	506.26	510.44	-35	4.18
Average Distance from Coastline (m)	463.73	472.51	479.57	**Average Migration Inland (m)**	7.06

(b) Punta Lobos - Row 323

Year	2007	2017	2037		
Simulated Depth (m amsl)	Simulated distance from coastline (m)			Simulated Depth (m amsl)	Evolution from 2017 to 2037 (m)
-2.5	382.81	393.00	422.07	-2.5	29.07
-7.5	399.22	408.43	440.08	-7.5	31.64
-12.5	411.39	419.58	452.88	-12.5	33.31
-17.5	420.66	431.55	462.49	-17.5	30.94
-25	432.34	442.75	471.50	-25	28.75
-35	445.09	455.34	488.99	-35	33.65
Average Distance from Coastline (m)	415.25	425.11	456.33	**Average Migration Inland (m)**	31.23

CHAPTER 5

DISCUSSION

5.1 Stable Isotopes

The resulting depleted values of $\delta^{18}O$ and $\delta^{2}H$ suggest that groundwater recharge is sourced by hurricane precipitation. Eastoe et al. (2015) identified a similar pattern of isotopic signatures in Todos Santos, and compared the results to groundwater sourced by monsoon precipitation. Monsoon precipitation and hurricanes are tropical depression rain events, and consistently produce rain with low $\delta^{18}O$ and $\delta^{2}H$ values (Eastoe et al., 2015). Eastoe et al. additionally found that the groundwater rapidly responds to different precipitation events, and concluded that groundwater is likely to originate as surface water in the low-elevation Todos Santos watershed. Samples plotting to the right and beneath the Global Meteoric Water Line (GMWL) show groundwater that has experienced evaporative effects, and La Poza's position indicates its composition is that of evaporated seawater.

Implications of these results are that groundwater originates in the lower elevations of the Todos Santos watershed as infiltration by precipitation sourced by hurricane events. Groundwater recharge is therefore dependent on the occurrence and frequency of these storms. When storms are less frequent and drought conditions exist, lowering of the water table is likely and can contribute to the exacerbation of seawater intrusion.

5.2 Specific Conductance

Specific conductance values published in 2007 and collected in 2017 exhibit spatial and temporal patterns which support interpretation that the aquifer is experiencing seawater intrusion.

Figure 12 shows the increase in specific conductance with proximity to the coast in both 2007 and 2017 data. Although well locations do not directly correlate from 2007 to 2017, areas of increased salinization over the 10-year period are identified, including wells within 1000 meters of the coastline and wells in close proximity to the lower reaches of Arroyo La Reforma. Highest values of specific conductance are located near the coastline, whereas lowest values are located furthest inland. The La Poza estuary displays a specific conductance of 74,400 uS/cm, nearly double that of seawater. This in combination with chemical analysis done in the area by Mahlknecht et al. (2018) indicate La Poza is comprised of evaporated seawater and consequently suggests the estuary receives little to no freshwater input, with the exception of surface runoff during precipitation events. Sample 07-9, which displays a specific conductance of 718 uS/cm in 2007 (Fig. 12) was taken from the lowest reach of Arroyo La Reforma. This reach was not flowing when the June 2017 field investigation took place, also suggesting that flow from La Reforma has been diverted, possibly by overexploitation of groundwater, and no longer serves as a freshwater source for La Poza.

Of additional concern is the location surrounding Samples 07-36 and 17-12 (Fig. 12). The measured head value of 07-36 in 2007 was -3 m amsl (CONAGUA, 2007). While more recent head measurements are unavailable, the water table elevation residing below mean sea level in 2007, combined with the increase in specific conductance (nearly doubled from 2007 to 2017) and the area's proximity to the coast, suggest the possibility of saltwater upconing.

5.3 Water Chemistry

Comparison of piper diagrams and HFE-D plots from 2007 to 2017 reveal significant aquifer water chemistry evolution over the 10-year span and spatially within the aquifer itself. The increase in chloride-type and sodium-chloride type water samples from 2007 to 2017 (Fig.

13) (Table 1) indicate an increase in chloride concentration of coastal areas within the aquifer. Chloride has been considered a conservative tracer of water salinization (Mahlknecht et al., 2018).

In the HFE-Diagrams (Fig. 14), according to Gimenez-Forcada (2010) the case of seawater intrusion is indicated by a rapid and distinct increase in salinity which almost simultaneously triggers the development of reverse exchange reactions, resulting in the composition CaCl, which has been abundantly associated with seawater intrusion (Stuyfzand, 1989) (Appelo & Postma, 2005). The proximity of 2007 sample positions to the trend line (Fig. 14a) represents simple mixing between freshwater and seawater, and is indicative of the aquifer being in a "recovery phase" (Giménez-Forcada, 2010). This suggests that, in 2007, the Todos Santos Aquifer may have been in a period of increased precipitation and henceforth increased freshwater recharge, which can additionally be inferred from the reported cumulative precipitation for years 2006 and 2007 (188.5 mm and 226.6 mm, respectively) (Tres Santos, 2012) as well as the thriving estuary in Figure 11a. Conversely, Figure 14b displays nearly all samples indicating the aquifer is in an intrusion phase. Notably, three samples are classified as NaCl-dominant, corresponding to the La Poza estuary and Las Palmas wetlands (surface water sources), and TS-20 (Punta Lobos, groundwater), defined as an evolution toward the seawater facies (Giménez-Forcada, 2010). Wells geographically located furthest inland (17-4, 17-5, 17-6, and 17-7) correspond to samples plotting in the early stages of intrusion and in the freshwater facies, whereas samples from water sources geographically located closest to the coastline (17-1, 17-19, 17-20) correspond to samples plotting in the late stages of intrusion and in the seawater facies. Multiple interpretations can be made from this temporal and spatial pattern. Seasonality can explain the freshening to intrusion difference between 2007 and 2017, as 2007 samples were

taken in November (winter, post rain season) and 2017 samples were taken in June (summer, pre rain season). Similar seasonal patterns are seen in Gimenez-Forcada's application of HFE Diagrams to a coastal aquifer in Spain (2010). This interpretation would suggest that the process of seawater intrusion is responsive to freshwater recharge. However, it further suggests that it is also exacerbated by prolonged drought periods, as seen from even the furthest inland 2017 samples being positioned in the intrusion phase (Fig. 14b). The location of samples positioned in the intrusion phase (Fig. 14) indicate wells as far inland as 1.9 kilometers in 2007 and as far as 2.9 kilometers in 2017 are affected by seawater intrusion. This combined with specific conductance trends (> 1000 μS/cm) suggest a mixing zone width in the Todos Santos area of approximately 1.4 kilometers in 2007, and a mixing zone width of approximately 2.4 kilometers in 2017. Seawater intrusion within coastal aquifers is a dynamic process, and any changes in the water balance can affect its location, at times resulting in alternation of recovery and intrusion phases. However, Lambrakis and Kallergis (2001) found that complete restoration of a freshwater aquifer after being subjected to seawater intrusion is practically impossible, making the consequences of prolonged drought periods on aquifer water quality effectively permanent.

Temporally, the combination of increase in percentages of chloride-type and sodium-chloride type water samples (Fig. 13), increase in mean specific conductance (Table 6), increase in percentage of samples exhibiting intrusion (Fig. 14), and decrease in percentage of samples exhibiting freshening (Fig. 14), together provide evidence that the water quality of the aquifer is degrading and furthermore is experiencing seawater intrusion of significant extent. Spatially, increases in chloride concentration and specific conductance with proximity to the coast in 2017 elicit the same interpretation.

5.4 Groundwater Modeling

5.4.1 Long-term Steady-State

The simulated mass balance for the long-term steady-state simulation provides insight into the dynamics of groundwater sinks and sources between growing and non-growing seasons. Groundwater recharge is provided in the lower topographic region of the Todos Santos watershed, concentrated in the valley of Arroyo La Reforma (simulated by RIV cells), with a lesser portion being sourced from upgradient inflow simulated by injection wells. Recharge from storm events is simulated by RIV cells, concentrated in the Todos Santos Valley. Groundwater is discharged principally by way of pumping.

5.4.2 Transient (2007-2017) Simulation

Model bias can be seen in the transient simulation, which attempted to reproduce concentration values collected in 2017 using results from the long-term steady-state simulation as initial conditions. Because of the challenges associated with calibrating to concentration values (Carrera et al., 2010), the decision was made to conserve long-term steady-state model parameters, as they were calibrated to hydraulic head values in addition to concentration values. The under-prediction of 2017 salinity conditions at depth should be noted when interpreting forecasting simulation results.

5.4.3 Forecasting Simulations

A sharp seawater-freshwater interface of 1.0 kg/m^3 is displayed in modelling results for display purposes, however, seawater-freshwater interfaces are typically defined by a mixing zone, rather than a sharp interface. Mixing zone width ranges widely between coastal aquifers (Lu et al., 2009). For example, Xue et al. (1993) found that the transition zone between seawater and freshwater in an alluvial aquifer off the coast of Laizhou Bay, China, varied from 1-6 km in

width, but was typically between 2 and 4 km. Therefore, this study utilizes the simulated location of the sharp interface in combination with chemical data in interpretation of the extent of seawater intrusion.

5.4.3.1 Scenario 1: Pumping and recharge remain constant

With no alterations made to model parameters, seawater intrusion is still evident, most significantly in the vicinity of Punta Lobos, where the seawater-freshwater interface reached 488.4 meters inland by 2037. A large initial increase in migration is seen from 2007 to 2017 in the Todos Santos area, explained by the initial doubling of extraction rates in all coastal and agricultural wells from the long-term steady-state to transient scenarios. Implications of this increase include the significant effect of increased pumping on seawater intrusion. In the vicinity of Todos Santos, while the seawater-freshwater interface only migrated an average of 0.7 meters inland between the years 2017 and 2037, it reached a maximum of 506.4 meters inland at the deepest layer (layer 6, simulated at -40 m amsl). Over the simulated 30 year period, the rate of intrusion resulted in approximately 0.32 meters/year for the Todos Santos vicinity and 1.32 meters/year in the Punta Lobos area. The rate of intrusion in the area of Punta Lobos increased from 0.99 meters/year between years 2007 and 2017 to 1.69 meters/year between 2027 and 2037. This result indicates that seawater intrusion is exacerbated in areas of the aquifer which are not in close proximity to La Reforma.

5.4.3.2 Scenario 2: Pumping is doubled in all wells, recharge remains constant

The simulated extent of interface migration in both areas with doubled pumping rates in all wells was similar to Scenario 1, however, migration of the seawater-freshwater interface further inland in the area of Todos Santos is still evident. The rate of intrusion increases slightly from Scenario 1.

5.4.3.3 Scenario 3: Pumping remains at 2017 conditions, sea-level rise of 4 mm/yr

The effect of sea-level rise on the seawater-freshwater interface is evident within the 20 year forecasting period. When compared with results from Scenario 1, the simulation of sea-level rise resulted in the seawater-freshwater interface migrating approximately 0.9 meters further inland in the Todos Santos area. In the Punta Lobos area, the interface migrated inland 0.4 meters further than in Scenario 1. Notably, the rate of intrusion is also increasing. From 2007 to 2017, the simulated rate of intrusion in the area of Punta Lobos was 0.99 meters/year, and increased to an average of 1.71 meters/year from 2027 to 2037. The rate of intrusion is highest in the lower-most layer of the model, reaching a rate of up to 2.15 meters/year between years 2027 and 2037.

5.4.3.4 Scenario 4: Pumping remains at 2017 conditions, La Reforma overexploited

Simulation of overexploitation of the lower reaches of Arroyo La Reforma had a significant effect on the extent of seawater intrusion in the Todos Santos vicinity. The simulated seawater-freshwater interface reached 514 meters inland in this area by 2037. The closest recorded well location is approximately 520 meters inland from the coastline in this area. The rate of seawater intrusion increased from 0.88 meters/year between years 2007 and 2017 to 1.39 meters/year between 2027 and 2037, with an average intrusion rate of 0.84 meters/year over the simulated 30 year period. Results did not change drastically in Punta Lobos from Scenario 1, further indicating La Reforma's negligible effect on the area. However, the rate of intrusion did increase between the years 2027 and 2037 from 1.69 meters/year in Scenario 1 to 1.73 meters/year. Results of this simulation show the significance of Arroyo La Reforma and the corresponding concentrated recharge in regards to the town's groundwater supply.

5.4.3.5 Scenario 5: Sea-level rise of 25 mm/yr

A worst-case scenario of sea-level rise was implemented for the 20 year forecasting model run to analyze the effect of extreme sea-level rise on the extent of seawater intrusion. Significant effects on seawater intrusion can be seen in the Todos Santos area, with a migration inland of nearly 7 meters from 2017 to 2037 and reaching a maximum of 510 meters inland. Notably, the simulated interface still does not reach as far inland as it does in Scenario 3, suggesting an even greater significance of La Reforma's presence on the extent of seawater intrusion.

For reference, the closest known well to the coastline in the area of Todos Santos is 17-12, at a distance of around 520 meters from the coastline. The simulated sharp position of the seawater-freshwater interface nearly reaches this far inland in forecasting simulations.

CHAPTER 6

CONCLUSIONS

Interpreted results from temporal and spatial specific conductance trends, temporal and spatial trends evident in major ion analysis, and variable-density groundwater flow modeling, all converge on the idea that the Todos Santos Aquifer is experiencing water quality degradation by salinization from seawater intrusion. The extent of intrusion is likely dynamic and varies with summer-winter seasons, precipitation, and rates of groundwater extraction.

Forecasting simulations indicate that the extent of seawater intrusion is exacerbated most severely by overexploitation of the main surface water catchment, Arroyo La Reforma. Arroyo La Reforma is a significant source of water for the Todos Santos Aquifer, provided it is connected to an upgradient subsurface water source, and is likely what has prevented the Todos Santos aquifer from experiencing the same extent of seawater intrusion as many of the surrounding aquifers in BCS. Recharge simulated by La Reforma in the model additionally takes into account the recharge provided by storm events, indicating the significance of infiltration by precipitation runoff, concentrated in the Todos Santos Valley, as a source of groundwater to the aquifer. Simulation of sea-level rise at the current rate of 4 mm/yr also had an appreciable, although less severe, effect on the extent of seawater intrusion. Forecasting simulation results suggest that seawater intrusion will continue into the future at a varying rate depending on: location within the aquifer, pumping rates, recharge rates, and surface water sources.

Increase of specific conductance values and chloride concentration values from 2007 to 2017 support the interpretation that groundwater near the coastline is being affected by seawater intrusion, however, seasonality differences between the time of year in which samples were

collected in 2007 and 2017 (November vs. June, respectively) may also contribute to the results seen. November of 2007 post-dated two above average precipitation years in Todos Santos, whereas June of 2017 was a time period characterized as mid-drought. The geographic location of samples displaying cation exchange reactions indicative of seawater-freshwater mixing support the interpretation that groundwater up to 1.9 kilometers inland was affected by salinization in 2007, and groundwater up to 2.9 kilometers inland was affected in 2017. This increase in affected groundwater is likely due to lack of freshwater recharge as a result of drought conditions.

Stable isotope analysis indicates groundwater is responsive to hurricane precipitation events, which recharge the aquifer in the lower topographic region of the watershed. This puts the aquifer at a significantly higher risk of permanent water quality degradation by seawater intrusion during prolonged periods of drought. Water demand increase as a result of expanding tourism, agriculture, and population growth, combined with prolonged drought periods will likely worsen this effect. Lambrakis and Kallergis (2001) concluded that, once groundwater experiences the relevant exchange processes exhibiting the intrusion phase, partial restoration of said groundwater can be achieved, but complete restoration is nearly impossible due to the long time period required. This implies that care should be taken with the goal of keeping the seawater-freshwater mixing zone to a minimum.

CHAPTER 7

RECOMMENDATIONS

Further field investigations would improve the current understanding of the groundwater dynamics in the Todos Santos Aquifer. Field data that could improve the current numerical model includes:

1. Aquifer geometry, specifically bathymetry, to better constrain groundwater flow processes. This could be done using various geophysical methods.
2. Recent hydraulic head and well depth measurements. Ideally, measurements could be taken in growing and non-growing seasons for multiple years. This would help constrain the aquifer's response to seasonal hydrologic stresses, including increased extraction by pumping wells and to periods of recharge by hurricane precipitation.

Further modeling work is recommended. Simulation of aquifer response to recharge in the form of cyclones, as well as varying recharge rates with time, would be beneficial. Numerical simulation of cation exchange processes would provide another level of detail in evaluating the extent of seawater intrusion.

Salinity ideally would be monitored in all aquifer wells to identify any further trends. Monitoring this during growing and non-growing seasons will assist in understanding how dynamic the seawater-freshwater interface is, and how its location and width responds to seasonal hydrologic stresses. This can be done by the local community's well owners with a conductivity probe.

A study on water transport infrastructure in Todos Santos would be greatly beneficial. CONAGUA (2007) recommended that surface water be utilized during drought periods so that

extraction doesn't affect the aquifer. Identifying the infrastructure needed to facilitate this would assist in preventing the exacerbation of seawater intrusion during drought periods.

LITERATURE CITED

Alfarrah, N., & Walraevens, K. (2018). Groundwater overexploitation and seawater intrusion in coastal areas of arid and semi-arid regions. *Water (Switzerland)*, *10*(2). https://doi.org/10.3390/w10020143

Anderson, M., Woessner, W., & Hunt, R. (2015). *Applied Groundwater Modeling: Simulation of Flow and Advective Transport*.

Appelo, C. A. J., & Postma, D. (2005). Geochemistry, Groundwater and Pollution. *Vadose Zone Journal*, *5*(1), 510. https://doi.org/10.2136/vzj2005.1110br

Calera, L. A., Mezquitillo, E., Guardia, C. L. A., Mar, J., Tunal, E., Mar, J., … Divisadero, C. E. L. (2001). Carta Geologico-Minera, Todos Santos F12-B33.

Cardona, A., Carrillo-Rivera, J. J., Huizar-Álvarez, R., & Graniel-Castro, E. (2004). Salinization in coastal aquifers of arid zones: An example from Santo Domingo, Baja California Sur, Mexico. *Environmental Geology*, *45*(3), 350–366. https://doi.org/10.1007/s00254-003-0874-2

Cardoso, P. R. (1993). Saline water intrusion in Mexico. *Transactions on Ecology and the Environment*, *2*, 37–43. https://doi.org/10.2495/AIR990911

Carrera, J., Hidalgo, J. J., Slooten, L. J., & Vázquez-Suñé, E. (2010). Problèmes conceptuels et de calibration des modèles d'intrusion marines. *Hydrogeology Journal*, *18*(1), 131–145. https://doi.org/10.1007/s10040-009-0524-1

Ceseña, F. M. R. (2015). Report of the current state of agriculture in Todos Santos and El Pescadero region 2015.

Chang, Y., Hu, B. X., Xu, Z., Li, X., Tong, J., Chen, L., … Ma, Z. (2018). Numerical simulation of seawater intrusion to coastal aquifers and brine water/freshwater interaction in south coast of Laizhou Bay, China. *Journal of Contaminant Hydrology*, *215*(29), 1–10. https://doi.org/10.1016/j.jconhyd.2018.06.002

CONAGUA. (2007). *Estudio para determinar la factibilidad de extraccion de agua subterranea salobre para su desalacion en los acuiferos de: Migrino Plutarco Elias Calles, El Pescadero, Todos Santos y Canada Honda, B.C.S.*

Craig, Harmon. (1961). Isotopic Variation in Metoeric Waters. *Science (New York, N.Y.). 133. 1702-3. 10.1123/science.133.3465.1702.*

Eastoe, C. J., Hess, G., & Mahieux, S. (2015). Identifying Recharge from Tropical Cyclonic Storms, Baja California Sur, Mexico. *Groundwater*, *53*(S1), 133–138. https://doi.org/10.1111/gwat.12183

Federman, D. K. (2015). *Segunda seccion secretaria de medio ambiente y recursos naturales*.

Fetter, C. W. (2001). *Applied Hydrogeology* (4th ed.).

Gelhar, L. W., Welty, C., & Rehfeldt, K. R. (1993). A Critical Review of Data on Field-Scale Dispersin in Aquifers - Reply. *Water Resources Research*, *29*(6), 1867–1869.

Giménez-Forcada, E. (2010). Dynamic of sea water interface using hydrochemical facies evolution diagram. *Ground Water*, *48*(2), 212–216. https://doi.org/10.1111/j.1745-6584.2009.00649.x

Guo, W., & D.Langevin, C. (2002). *User ' s Guide to SEAWAT : A Computer Program For Simulation of Ground-Water Flow Techniques of Water-Resources Investigations of the U . S . Geological Survey User ' s Guide to SEAWAT : A Computer Program for Simulation of Three-Dimensional*.

Harbaugh, A. W., Banta, E. R., Hill, M. C., & McDonald, M. G. (2000). MODFLOW-2000 User guide to modularization concepts and the Ground-Water Flow Process. *U.S. Geological Survey Open-File Report 00-92, 121 P.*

Hill, M. C., Banta, E. R., Harbaugh, A. W., & Alderman, E. R. (2000). MODFLOW2000, the U.S. Geological Survey modular ground water model user guide. *U.S. Geological Survey Open-File Report*.

INEGI. (n.d.). Instituto Nacional de Estadistica y Geografia (INEGI). Retrieved from https://www.inegi.org.mx/

Kooiman, I. J. W., Stuyfzand, P. J., Maas, C., & Kappelhof, J. W. N. M. (2004). Pumping brackish groundwater to prepare drinking water and keep salinizing wells fresh: A feasibility study. *Proceedings of the 18th Salt Water Intrusion Meeting*, 625–635.

Langevin, C. D., Thorne, D. T., Dausman, A. M., Sukop, M. C., & Guo, W. (2008). SEAWAT Version 4: A Computer Program for Simulation of Multi-Species Solute and Heat Transport: U.S. Geological Survey Techniques and Methods Book 6, Chapter A22, 39.

Lewis, E. L. (1980). The Practical Salinity Scale 1978 and Its Antecedents. *IEEE Journal of Oceanic Engineering*, *OE-5*(1), 3–8.

Lin, J., Snodsmith, J. B., Zheng, C., & Wu, J. (2008). A modeling study of seawater intrusion in Alabama Gulf Coast, USA. *Environmental Geology*, *57*(1), 119–130. https://doi.org/10.1007/s00254-008-1288-y

Lu, C., Kitanidis, P. K., & Luo, J. (2009). Effects of kinetic mass transfer and transient flow conditions on widening mixing zones in coastal aquifers. *Water Resources Research*, *45*(12). https://doi.org/10.1029/2008WR007643

Mahlknecht, J., Sanford, W. E., Fichera, M., & Mora, A. (2018). Freshwater-seawater transition in coastal Todos Santos aquifer, Baja California Sur. *Energy Procedia*, *153*, 191–195. https://doi.org/10.1016/j.egypro.2018.10.059

Narayan, K. A., Schleeberger, C., & Bristow, K. L. (2007). Modelling seawater intrusion in the Burdekin Delta Irrigation Area, North Queensland, Australia. *Agricultural Water Management*, *89*(3), 217–228. https://doi.org/10.1016/j.agwat.2007.01.008

NASA. (n.d.). Satellite sea level observations. Retrieved from https://climate.nasa.gov/vital-signs/sea-level/

Roberto Carmona, Gerardo Marrón, Adriana Hernández Alvarez, Abigail Rivas, G. D. D. (2017). Propuesta para la designación de los oasis “La Poza” y “San Pedro del Palmar”, Todos Santos, Baja California Sur, como Áreas de Refugio para Proteger Especies Acuáticas, con base en su relevancia para la Mascarita peninsular (Geothlypis beldingi), (1).

Rumbaugh, J., & Rumbaugh, D. (2011). Groundwater Vistas version 6. *Environmental Simulations, Inc.*

SAGARPA. (n.d.). Secretaria de Agricultura y Desarrollo Rural. Retrieved from https://www.gob.mx/sader

Scheidleder, A., & Grath, J. (2004). Saltwater intrusion due to groundwater over-exploitation - EEA inventory throughout Europe. *Swim*, (June), 125–126.

Stuyfzand, P. J. (1989). A new hydrochemical classification of water types, (182), 89–98.

Tamez-Meléndez, C., Hernández-Antonio, A., Gaona-Zanella, P. C., Ornelas-Soto, N., & Mahlknecht, J. (2016). Isotope signatures and hydrochemistry as tools in assessing groundwater occurrence and dynamics in a coastal arid aquifer. *Environmental Earth Sciences*, *75*(9). https://doi.org/10.1007/s12665-016-5617-2

Tres Santos. (2012). *Geo-Hydrological Synopsis of the Todos Santos Aquifer*.

USGS. (2016). Saline Water. Retrieved from http://water.usgs.gov/edu/saline.html

Walther, M., Delfs, J. O., Grundmann, J., Kolditz, O., & Liedl, R. (2012). Saltwater intrusion modeling: Verification and application to an agricultural coastal arid region in Oman. *Journal of Computational and Applied Mathematics*, *236*(18), 4798–4809. https://doi.org/10.1016/j.cam.2012.02.008

Zheng, C., & Wang, P. (1999). MT3DMS: A modular three-dimensional multispeces transport model for simulation of advection, dispersion, and chemical reactions of contaminants in groundwater systems. Technical report, Waterways Experiment Station, US Army Corps of Engineers. *A Modular Three-Dimensional Multi-Species …*, (June), 239.